University of Nevada, Reno

The Development and Optimization of Raman Spectroscopy Analyses for Mobile Salinity Sensing

A thesis submitted in partial fulfillment of the
requirements for the degree of Master of Science in
Mechanical Engineering

by

Amanda K. Nelson

Dr. Eric L. Wang/Thesis Advisor

May, 2017

THE GRADUATE SCHOOL

We recommend that the thesis
prepared under our supervision by

AMANDA K. NELSON

Entitled

The Development and Optimization of Raman Spectroscopy Analyses for Mobile Salinity Sensing

be accepted in partial fulfillment of the
requirements for the degree of

MASTER OF SCIENCE

Eric Wang, Ph. D., Advisor

Pradeep Menezes, Ph. D., Committee Member

Jeffrey LaCombe, Ph. D., Graduate School Representative

David W. Zeh, Ph.D., Dean, Graduate School

May, 2017

Abstract

To quantify the amount of deicing salt on the roadway in near-real time, this thesis proposes a mobile salinity sensor using Raman spectroscopy. This thesis investigates the viability of using Raman spectroscopy to determine the concentration of salt deicer in an aqueous solution in near-real time through a two part study. The first portion describes the use of Raman spectroscopy to determine the concentration of aqueous solutions consisting of the five most common salt deicers: sodium, calcium, and magnesium chloride, potassium acetate, and calcium magnesium acetate. The Raman spectra are analyzed using previously established methods for determining chloride salt concentration that were optimized to work with both acetate and chloride salt solutions. These analyses output a benchmark plot for each salt solution over a range of concentrations and temperatures. The second portion of this study focuses on characterizing the effect that the testing surface substrate has on the concentration found from the Raman spectrum of the sample. This was completed by recording the Raman spectrum on a variety of surfaces with multiple surface treatments. The results were compared to the benchmark plots previously determined. Using the optimized analysis methods and the ideal surface found via this study, a mobile salinity sensor using Raman spectroscopy can be designed to work consistently and accurately in near-real time.

Dedication

To Mom and Dad.

Acknowledgements

I would like to take this opportunity to formally thank my advisers, Dr. Eric Wang and Dr. Jeffrey LaCombe, for the support and direction they provided throughout this study. This thesis was only possible because of the guidance that they provided. I would also like to thank my lab mate João Paulo Braz for his advice and questions that allowed me to discover new areas of my research. I would like to acknowledge the funding provided by the Federal Highway Administration and the Nevada Department of Transportation. Additionally, I would like to thank Dr. Pradeep Menezes for his participation in my graduate committee.

I would like to thank Dr. Dev Chidambaram for the use of his DXR Raman Microscope, fiber optic probe, and laboratory space while I collected my data, and Dr. Augustus Merwin for his guidance and instructions on Raman spectroscopy methods. Additionally, I would like to acknowledge Zachary Karmiol and William Phillips for their assistance in gathering initial measurements and opening the laboratory for me to use.

Lastly, I would like to thank my mom and dad, Doug Menozi, and the rest of my family for their patience and support as I spent my time working on this project.

Contents

List of Figures

List of Tables

Nomenclature:

$CaCl_2$: Calcium chloride

CMA : Calcium magnesium acetate

DOT : Department of Transportation

FHWA : Federal Highway Administration

FWHM : Full width at half maximum

ICP-MS : Inductively coupled plasma mass spectrometry

JH : Japan Highway Public Corporation

KAc : Potassium acetate

MDOT : Maryland Department of Transportation

MDSS : Maintenance decision support system

$MgCl_2$: Magnesium cloride

MnDOT : Minnesota Department of Transportation

NaCl : Sodium chloride

NDOT : Nevada Department of Transportation

R_A : Ratio of the areas

R_a : Average surface roughness

Chapter 1

Introduction

1.1 Motivation

Transportation agencies spend considerable amounts of resources each year to maintain safer winter driving conditions; however, many state agencies face strict budget constraints and backlash from the public on the environmental effects of current snow and ice removal techniques. Over the last five years, the Nevada Department of Transportation (NDOT) has spent an average of $6 million annually to remove snow and ice from over 5,000 miles of roadways [1–5]. Additionally, as much as 11% of NDOT's overall materials budget is devoted to salt and sand each year to create safer winter driving conditions. Though NDOT allocates a significant amount of monetary and physical resources each year to winter maintenance efforts, other transportation agencies in areas subjected to harsh winters, such as Minnesota DOT and Maryland DOT, or with more miles of maintained roads can spend upwards of $98 million annually on snow and ice removal [6–8]. A portion of the transportation agencies implementing chloride salt based deicers have noted damage to trees and structures in areas where

the deicer has been applied due to the corrosive nature of chloride based salts [9, 10]. While large budgets can create safer driving conditions, transportation agencies have an obligation to reduce both their expenditures and the environmental impact of their deicing methods.

To reduce the environmental impact and structural damage that chloride based deicing salts can cause, many transportation agencies have begun using acetate based deicing salts; however, these acetate salts are more expensive than chloride based deicing salts. In 2010, acetate salts cost from 10 to 40 times more per ton than chloride deicing salts [11]. Because these "environmentally friendly" salts cost significantly more, the amount of material applied to the roadway must be monitored.

In conclusion, whether a transportation agency applies chloride or acetate based deicing salts, a system must be used to determine the amount of deicer in use to prevent over-salting which will mitigate the environmental impact and budget impact.

1.2 Thesis Objectives

The goal of this project was to assess the viability of using Raman spectroscopy to determine the concentration of salt deicer on the roadway from a vehicle mounted mobile salinity sensor in near-real time. The objectives of this thesis were as follows:

1. Develop a method for determining the concentration of all five of the most common salt deicers consistently by building on existing methods and optimizing the method to produce results in near-real time.

2. Characterize the Raman spectrum for a deionized water solution placed on a variety of surfaces with different textures.

3. Generate benchmark plots showing the relationship between a scalar represen-

tation of the Raman spectrum, temperature, and concentration for all five of the most common salt deicers.

1.3 Summary of Completed Work

The work completed in this thesis was performed to guide the design phase for a Raman spectrometer mobile salinity sensor. Previously published methods for determining the concentration of chloride salt solutions were optimized to accurately and efficiently determine the concentration of both acetate and chloride salt solutions. From the optimized method, benchmark plots were created for all five of the most common salt deicers. Using the benchmark plots, the effect of the testing surface on the collected Raman spectrum was determined. Stainless steel surfaces were tested with a variety of surface treatments in order to create a working list of useful surface preparations for the test plate of the mobile salinity sensor. With the analysis optimized and a list of useful surfaces started, the design of the mobile salinity sensor can more easily follow.

1.4 Thesis Organization

This thesis was completed to investigate the viability of using Raman spectroscopy to determine the concentration of salt deicer on the roadway in near-real time. This was done by showing that Raman spectroscopy can be used to determine the concentration of aqueous solutions with various chemical makeups and by determining what surfaces can be used to achieve clear results. Since this project is a crossover between two disciplines, an extensive background on current winter roadway maintenance systems, the theory behind Raman spectroscopy, and the current applications of Raman

spectroscopy in related areas are provided in Chapter 2. Additionally, a discussion of the current state of technology for determining roadway salt deicer concentrations is included. Chapter 3 describes the methodology for the solution characterization tests used to determine the viability of using Raman spectroscopy to determine the concentration of samples containing one of the five most common salt deicers. The sample and test setup as well as the data analysis techniques are also included in this section. Chapter 4 details the methodology for collecting the Raman spectrum of deionized water samples on stainless steel surfaces with various surface treatments performed to reduce fluorescence of the sample. The results from both the sample tests and the surfaces tests are presented in Chapter 5. These figures include the benchmark plots of the results achieved from optimizing the Raman spectra data analysis. The conclusions drawn from this project are outlined in Chapter 6 while areas with potential for future work are detailed in Chapter 7.

Chapter 2

Background

2.1 Winter Road Maintenance

Transportation agencies in areas subjected to harsh winter weather conditions dedicate considerable amounts of resources to snow and ice removal annually to create safer winter driving conditions. In the United States, approximately 70% of maintained roads are in areas subjected to five or more inches of snow annually [12]. Several state and local transportation agencies are tasked with maintaining the roadways through various anti- and decing methods. In 1991, the National Research Council estimated that the United States spent around $1.5 billion each year on highway snow and ice control with roughly a third of the budget devoted to chemical deicing agents [13]. The Federal Highway Administration (FHWA) now estimates that more than $2.3 billion are spent annually by state and local transportation agencies on snow and ice control efforts [12]. Despite these efforts, 1,300 people are killed annually in the United States in vehicular accidents caused by precipitation covering the roadway [12].

In addition to vehicular accidents, many researchers have hypothesized that the deicing measures put forth by transportation agencies also create a level of harm to the environment. Many concerned research groups have put forth effort in analyzing the effect that deicing salts have on the environment [9,14–16]. In the Reno area, a portion of these studies focus around the loss of trees in the Lake Tahoe basin [9, 16]. One research group found elevated chloride levels in waterways near roadways subjected to chloride salt deicers [9]. This was a cause for concern because previous studies had suggested a link between elevated chloride levels and tree loss; however, further review showed that the chloride itself does not cause permanent damage to the trees [16]. Instead, the chloride weakens the tree's natural defenses which makes them more prone to damage from insects and micro-organisms [16]. Upon showing this, the study hypothesized that trees subjected to high chloride levels could recover when the water chloride levels were reduced. This precipitated the call for preventing over-salting of the roadways from an environmental perspective.

In an effort to ensure proper snow and ice control methods are implemented across the country to reduce vehicular accidents and environmental impact, in 1996 the Federal Highway Administration (FHWA) released a manual on effective anti-icing techniques [17]. The manual outlines when and how to apply the most common deicing salts, sodium (NaCl), calcium ($CaCl_2$), and magnesium chloride ($MgCl_2$), potassium acetate (KAc), and calcium magnesium acetate (CMA). Since each salt deicer has different chemical properties and varying effects on the melting point of ice, the manual lists which salt to use for each expected temperature and how to prepare an effective solution. The manual provides information for each state department of transportation, DOT, or other local transportation agencies on how to tailor the anti-icing program to the local conditions and climate, agency resources, and desired level of service. The following subsections outline how NDOT and other DOT's across

the country have implemented the information in this manual to suit their location.

2.1.1 NDOT

The Nevada Department of Transportation (NDOT) expends considerable monetary and physical resources each year to remove ice and snow from over 5,000 miles of roads to create safer winter driving conditions. These snow and ice removal efforts have cost an average of $6 million annually over the last five years with up to 11% of the total material budget spent on deicing salt and sand [1–5]. In spite of NDOT's preventative measures, over 2,000 vehicular accidents occur statewide with snow, ice, and wet roadway conditions reported as the cause [18]. Because of this, NDOT is constantly looking to improve their anti- and deicing methods while reducing their overall snow and ice removal costs so that the budget can be allocated elsewhere.

NDOT currently employs multiple chemical salt deicers to aid with both ice and snow removal and anti-icing procedures. For general anti-icing procedures, NDOT applied a 23% salt brine solution directly to the roadway to prevent ice from bonding to the roadway surface, as recommended by the FHWA [12, 18]. This salt brine solution is crafted from rock salt or commercial grade NaCl with a maximum of 5% impurities and is recommended for roadway surface temperatures as low as -21 °C [12]. Deicing measures often require salt solutions with lower eutectic points (the lowest freezing point temperature for a solution) than NaCl solutions can provide. In this case, NDOT has elected to use $MgCl_2$ or KAc solutions [18,19]. These deicing solutions are dispensed through automatic deicing systems embedded in the pavement activated remotely that spray the solution directly onto the roadway; however, NDOT has only placed these systems on bridges as of yet, which means salt/sand spreaders are still used to deice additional portions of the road [18]. In addition to chemical deicing solutions, NDOT commonly spreads salt and sand mixtures on the roadway with de-

icing solutions sprayed over the top of the mixture to create a dense layer to provide traction while the ice melts. All of these methods combine to make the roadways safer in winter conditions, but NDOT desires to be able to determine the concentration of salt already on the roadway to ensure the correct mixture is applied for effective anti-icing without wasting material or creating unnecessary environmental stress.

2.1.2 Other DOT's

While Nevada is known for hazardous winter weather conditions, especially in the Sierra Nevada Mountain passes, there are other states that require larger budgets and more resources to keep their roadways safe in winter conditions. The Maryland Department of Transportation (MDOT) spent over $87.9 million in snow and ice removal last year [6, 7], and the Minnesota Department of Transportation (MnDOT) spent over $98.5 million on average for snow and ice removal each year over the last five years [8]. The snow and ice removal budgets cover equipment, material, and labor costs [8]. In addition to having more miles of roadway to service and more frequent winter weather conditions as compared to Nevada, these DOTs and other transportation agencies devote significantly larger monetary resources to snow and ice removal because of their use of acetate and chloride deicing salts chosen to replace rock salt. While these alternative deicing salts lower the freezing point of the precipitation beyond what rock salt can achieve, the acetate salts can cost anywhere from 10 to 40 times more per ton than chloride salts [11]. In addition to costing more, the FHWA noted that the acetate solutions require a higher concentration to reach their eutectic concentration (concentration producing the lowest freezing point) as compared to the chloride salt solutions [12]. Since these alternative salts are often required because of the low temperatures these areas experience, each DOT must determine an effective method for controlling their deicing salt application to maintain their budgets while

providing the best service possible for their constituents.

To reduce expenditures and preserve the environment, multiple DOTs have implemented systems to optimize their use of chemical and physical deicing agents. A Maintenance Decision Support System (MDSS) is often employed by state and local transportation agencies to manage the use of snow and ice removal resources and allows agencies to plan for and apply necessary roadway treatments when they are needed [20]. With this system in place, the transportation agencies can ensure that they are only applying deicing salts to the roadway when required. While the MDSS can advise on whether or not an anti-icing solution is necessary, it cannot quantify the amount of deicing salt currently on the roadway; therefore, there is a need for a system to determine the concentration of salt solutions on the roadway in real time to help prevent over-salting.

2.2 State of Technology

Hand-held salinity sensors have been used for years in environmental studies to determine the amount of salt in bodies of water or in plant life [21]; however, various transportation agencies and researchers in recent years have developed means for measuring the concentration of deicing salt on the roadway remotely. A few of these methods have been designed as stand-alone systems while others have been implemented in parallel to provide the best service. While no technology currently exhibits widespread use, the following roadway salinity sensors are some of the most commonly used systems currently under investigation or employed at this time.

2.2.1 In-Road Precipitation Sensor Units

Transportation agencies commonly embed sensors in the roadway surface to accurately determine roadway conditions and use the information to improve the roadway. One such sensor that can be implemented is an in-road precipitation sensor that detects the presence and phase of precipitation on the roadway which in turn gives information about the concentration of the solution. Most commonly, these in-road devices incorporate sample wells to collect a small sample of precipitation from the roadway to run tests on, though the methods in which the tests are performed can vary [22, 23].

Whitener designed an in-road sensor capable to determining the depth and current phase of precipitation (liquid, snow, etc.) on the roadway in real time [22]. Using an electrode and a sensor, an electric current is passed through the collected sample and varied with time. The conductive losses between the sensor and electrode reveal the amount of precipitation collected in the sample well and the presence of impurities. Unfortunately, this method does not directly calculate the salt concentration in the solution.

Leonhardt and coworkers built upon Whitener's designs by allowing the system to determine the concentration of deicing salt in the precipitation sample via the use of a conductivity probe [23]. Knowing the type of salt that the transportation agency applies to the roadway, the conductivity reading can determine the concentration of the solution. Leonhardt and coworkers then programmed the unit to calculate the approximate freezing point of the precipitation on the roadway to alert transportation agencies. Though this sensor is stationary and cannot read the salt concentration of the entire roadway, it has the benefit of sending the freezing point, salt concentration, and temperature information digitally. This means that the device can be used remotely to sense whether the roads need additional salt or sand applied to combat

hazardous conditions.

Clearly, in-road precipitation sensors can calculate the concentration of deicer on the roadway by analyzing the phase of the precipitation collected on the roadway when the temperature of the sample is known. Unfortunately, this method becomes complicated when multiple deicing salts are present and other impurities, such as sand, are found in the solution.

2.2.2 Conductivity Probes

As an alternative to in-road precipitation sensors, some researchers have developed mobile salinity sensors using conductivity sensors to determine the concentration of salt on the roadway. Handheld conductivity sensors have been used for environmental studies for years to determine the effect of road salt on the environment [21], but Garrick and coworkers designed an on-vehicle mobile salinity sensor capable of reading the concentration of aqueous chloride salt solutions on a roadway [24].

Garrick and coworkers' setup features a collection box mounted behind the tire wheel well in order to collect tire splash from the roadway. The design uses a heater to ensure that the sample is in liquid form and relies upon a thermometer to determine the temperature of the sample since the conductivity reading can be altered by the temperature [24]. The tire splash is then collected, and 66 mL volume of roadway sample must be retained to measure the conductivity of the sample.

At slow speeds, Garrick and coworkers' design takes an average of 26 seconds to collect and measure the conductivity of the sample [24]. This means that results can be seen in near-real time. While the speed of their system is impressive, conductivity probes have difficulty determining the concentration of some acetate salt solutions on the roadway because of the low molar conductivity that the acetate ions provide [25].

2.2.3 Laser spectroscopy

Both the in-road precipitation sensors and the conductivity probe system rely on liquid roadway salt samples to determine the concentration of salt on the roadway; however, many transportation agencies would like to determine the amount of dry residual salt on the roadway to determine an effective anti-icing concentration to apply without over-salting. Researchers like Ruiz-Llata and coworkers and the Japan Highway Public Corporation (JH) have employed the use of laser spectroscopy to quantify the concentration of residual salt on the roadway [26, 27].

In order to evaluate the concentration of residual dry salt on the roadway, Ruiz-Llata and coworkers implemented a system for sensing concentration directly from the roadway instead of collecting samples from the tire splash of the vehicle when the vehicle is in motion [26]. An on-vehicle fluorimeter was used to achieve this. The fluorimeter recorded the fluorescence of the roadway and compiled the data into excitation-emission maps that can be used to determine the concentration of salt on the roadway in near-real time [26]. The results of the tests allowed Ruiz-Llata and coworkers to determine that temperature does not affect the fluorescence readings. With these findings, Ruiz-Llata and coworkers determined that their system could accurately determine the concentration of dried salt deicer on the roadway without knowledge of the roadway temperature. However, they admitted that their design would have to be altered to read directly from the roadway since the experimental setup required a smaller focal distance between the fluorometer probe and the sample than would be possible for a real world system.

While Ruiz-Llata and coworkers designed their system to read the residual salt concentration by shining the sensor directly on the roadway, the JH used the tire splash method commonly used to gather conductivity measurements [27]. Like Ruiz-Llata and coworkers found, dry salt particles on the roadway are not easily collected

remotely from the tire splash of the vehicle. To reliably collect the sample, the JH designed a system in which a known amount of water is sprayed on the roadway in front of the tire. The residual salt is collected in an aqueous form and the concentration is analyzed using laser spectroscopy. For the JH, a near-infrared LED was used to determine the refractive index of the sample which was used to calculate the concentration of the dry residual salt on the roadway.

While the laser spectroscopy studies discussed here were aimed at analyzing the dry residual salt remaining on the roadway after a winter storm or prior to application of new material, the JH showed that laser spectroscopy works for aqueous solutions as well. From these spectroscopy studies, using Raman spectroscopy to analyze the concentration of an aqueous solution with a known chemical makeup emerges as an intriguing alternative.

2.3 Raman Spectroscopy

Raman spectroscopy has been used for years in environmental studies to determine the concentration of salts in natural bodies of water [28,29] or in the soil [30]. Because Raman spectroscopy has been proven effective in determining the concentration of salt in environmental studies, we propose applying this technology to determine the concentration of salt on the roadway in near-real time. Raman spectroscopy has many advantages that make it a viable option for a mobile salinity sensor. The following sections explain the theory behind Raman spectroscopy as well as providing information on the Raman spectrum for pure water and how the spectrum in currently used to determine the salt concentration in a solution.

2.3.1 Theory

To percieve the appeal of using Raman spectroscopy as a mobile on-vehicle salinity sensor, what sets it apart from other forms of spectroscopy must be understood. There are many types of spectroscopy, but all spectroscopic methods use radiated energy to detect molecular vibrations which can be used to identify a substance and its concentration in a sample [31]. Since Raman spectroscopy is a sub-category of laser spectroscopy, all general discussions in this section will focus on properties of laser spectroscopy methods.

Laser spectroscopy methods use a laser of a known wavelength as the radiated energy source and rely on the interactions with the laser beam and the sample to determine the phase and chemical makeup of the sample. In order to determine the current phase and chemical makeup of a sample from its molecular vibrations, the way molecules behave under the influence of photons, must be understood. At room temperature, most molecules in a sample are present at the lowest energy vibrational level, m, as shown in Figure 2.1 (Stokes, Rayleigh, and anit-Stokes are described later in this section) [31]. When light photons interact with matter, the photons may be absorbed, scattered, or pass through the sample without interacting. When the light photons interact with the molecules in a sample, the molecules' electron cloud becomes polarized which creates an unstable and temporary virtual state (Fig. 2.1). Since virtual states are created when the laser photons interact with electrons in the molecules, the energy level of these virtual states is determined by the wavelength of the laser source used. At the end of this temporary state, the light photon is re-radiated from the molecule, and the molecule returns to ground vibrational state, m, or a slightly elevated vibrational state, n (Fig. 2.1). The temperature of the sample must be noted prior to testing because thermal energy may elevate some molecules to an excited state such as n in Figure 2.1 which causes the molecules to have a slightly

different interaction with the incoming photon as compared to molecules at the lowest energy vibrational state, m.

When an excitation laser is applied to a sample and re-radiated, three forms of scattering can occur: Stokes, Rayleigh, and anti-Stokes. Rayleigh scattering occurs when the molecule starts and ends at the same vibrational state which elastically scatters the light as shown in Figure 2.1 [31]. Rayleigh scattering produces a strong signal because it occurs in most photons. Raman scattering is composed of both Stokes and anti-Stokes scattering. Stokes scattering occurs when the molecule absorbs energy from the excitation laser photon while anti-Stokes scattering results from energy being transferred from the molecule to the photon as it is scattered [31]. Because Raman scattering analyzes the inelastic changes in the photon energy, it uses a slightly different technique for determining the molecules in a substance.

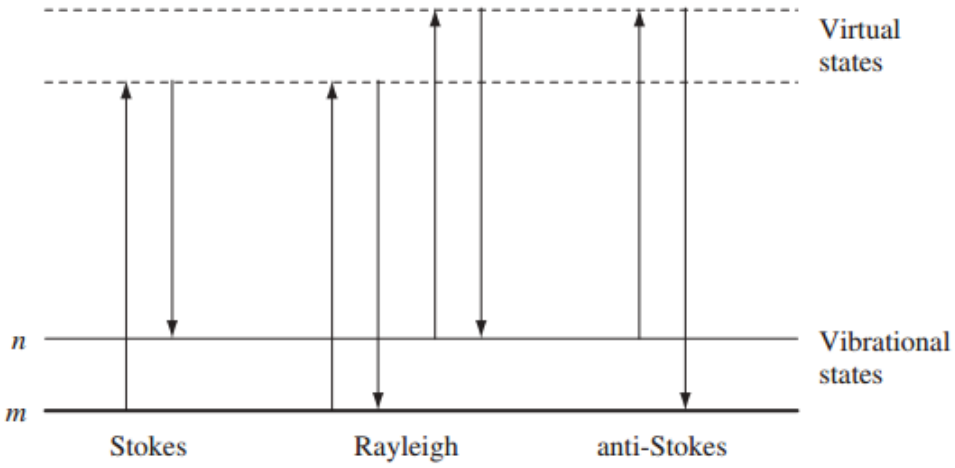

Figure 2.1: Pictorial representation of energy states of a molecule and how they change when under the excitation of a laser [31].

While the various methods of laser spectroscopy all use a laser light source to create molecular vibrations, Raman spectroscopy is unique in the way the molecular vibrations are analyzed. Raman spectroscopy is performed by shining a monochromatic excitation laser on a sample [32] and recording the Raman scattering in the

reflected beam. Raman scattering arises from a change in the polarizability of a molecule produced when energy is transferred from either the photon of the excitation laser to the molecule or from the molecule to the scattered photon [31]. From this, Raman scattering can be separated into two processes: Stokes and anti-Stokes scattering. Stokes scattering occurs when a molecule starts at the ground vibrational state,m. The molecule reaches a virtual state when exposed to the excitation laser photons and absorbs a portion of the photon energy that leaves the molecule at an excited vibrational state, n, when the photon is re-radiated from the molecule (Fig. 2.1). Anti-Stokes scattering occurs when a molecule starts at an elevated vibrational energy state, n, and is exposed to an excitation laser photon. When the photon is re-radiated, the molecule transfers energy to the scattered photon which drops the molecule to the ground vibrational energy state, m (Fig. 2.1). As the frequency of the molecular vibrations increase, Stokes scattering will begin to overpower the anti-Stokes scattering. This is the reason why most papers, including this one, only record the Stokes scattering. A third form of scattering is also present, Rayleigh scattering; however, most spectrometers use a filter to remove the Rayleigh scattering along with the light reflecting at the same wavelength as the excitation laser so that the weak Raman peaks can be seen in the final spectrum [31].

The weak Raman scattering can identify a molecule because molecules with different numbers of atoms and geometry will experience varying responses to an excitation laser. Triatomic molecules, like water, experience three vibrational modes when subjected to an excitation laser: symmetric stretching, asymmetric stretching, and bending [31]. Symmetric stretching causes large polarization changes in the molecules and strong Raman scattering results. The bending vibration mode causes little polarization change which causes weak Raman scattering. Since the symmetric stretching vibrations provide the most Raman scattering, the stretching region of the

water Raman spectrum is the focus of most studies involving aqueous salt solutions because of the exaggerated effects of the salt ions in this region. However, to focus on this region, the Raman spectrum of the sample must first be collected.

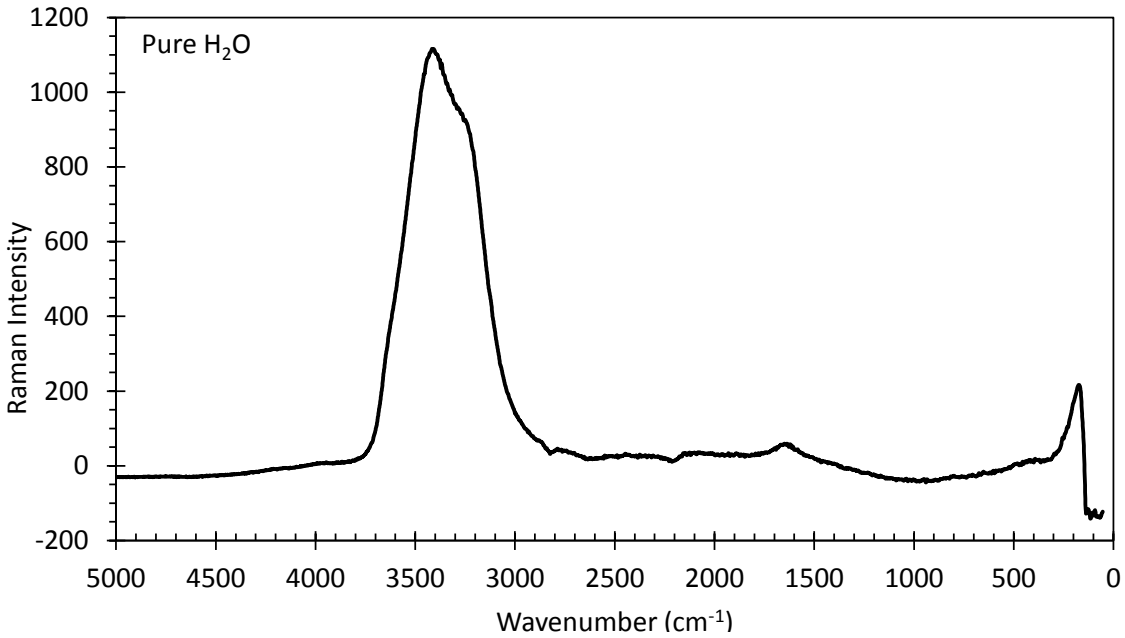

Figure 2.2: Raman spectrum for deionized water recording the changes in photon energy emitted by the exictation laser and the light scattered from the sample.

The Raman spectra are created by measuring the difference between the photon energy of the excitation laser and the photon energy of the scattered or reflected beam created after radiating the sample [33]. The change in energy is a wavenumber that corresponds to a line or band on the Raman spectrum [32]. The x-axis has units of wavenumbers (cm^{-1}) (Fig. 2.2), though the x-axis values are actually equal to the shift in energy from the excitation laser wavenumber to the wavenumber value of the scattered beam [31]. The y-axis of the Raman spectrum corresponds to the Raman intensity of the received signal (Fig. 2.2) which is determined by the number of collected photons involved at each energy level [33]. The Raman spectra are generally plotted with the wavenumbers increasing to the left though this is more of

a guideline than a rule [32, 33]. Once the Raman spectra are collected, the spectra are often normalized to the same Raman intensity at a chosen point for comparison purposes. This ensures that the relative intensities for the spectra remain the same while allowing for changes in the spectra to be seen more clearly.

2.3.2 Application of Raman Spectroscopy

Like many spectroscopy methods, Raman spectroscopy is capable of analyzing aqueous salt solutions, but Raman spectroscopy has a few advantages that make it preferable for a mobile salinity sensor. Compared to other spectroscopic methods, Raman spectroscopy requires comparitively less expensive equipment to perform [32]. Additionally, it can analyze a small volume of sample of a known temperature without contacting the sample. These are all advantageous because the deicing salts can be corrosive [10], and large sample volumes take longer to collect via the common tire splash method. A critic might remark on the disadvantages of Raman spectroscopy at this point, but there are methods of reducing the impact of those disadvantages.

Because Raman spectroscopy relies on the vibration of molecules to determine the chemical makeup of the sample, dissolved salts cannot be characterized directly from the Raman spectrum of an aqueous solution. Instead, the effect of salt ions on the water molecule's Raman spectrum can be analyzed to determine the concentration of salt in the surrounding solution. Various methods have been developed to determine the change in the water Raman spectrum created by salt ions, but the behavior of the pure water Raman spectrum must be understood before these methods can be implemented.

For a Raman spectrometer to work as a mobile salinity sensor, a fiber optic probe is most effective for collecting the Raman spectra of the samples. This creates additional issues because excitation lasers are known to excite Raman scattering from the fiber

optic material itself. The Raman scattering from this leads to fluorescence powerful enough to override the weak Raman scattering of the sample [31]. Manufacturers of these fiber optic probes have decreased this effect by emitting the excitation laser from a series of fibers around the outside of the probe and collecting the resulting scattered photons through a single fiber strand in the center of the probe. By doing this, most researchers will only experience large levels of fluorescence when a large volume of light is scattered. Therefore, reducing the laser power to decrease the amount of light the probe collected will reduce the chances of fluorescence of the fiber optic material.

Of the many spectroscopic methods, Raman spectroscopy is often considered less popular because it produces weaker signals and can have samples experience fluorescence which can alter the resulting Raman spectrum; however, multiple methods have been developed to counteract these disadvantages. Raman scattering only occurs for one in every 10^6 to 10^8 photons that are scattered which provides opportunities for fluorescence and signal noise to alter the Raman spectrum [31]. To improve the Raman signal, a few techniques have found that using a shorter sample time when collecting the Raman spectra decreases the chance for noise to occur in the data [33]. Additionally, since the intensity of Raman scattering is related to the power of the laser used to excite the scattering, the highest frequency excitation laser possible should be used to improve the Raman scattering relative to the fluorescence contribution [31]. Most researchers choose an excitation laser in the visible light region to reduce the chances of the laser being absorbed by the sample or of the heat damaging the sample. The fluorescence created by choosing a laser in the visible light region can be decreased by turning down the power of the laser and by choosing a testing surface that does not fluoresce. In summary, by implementing a higher wavenumber laser with a shorter sample time and a testing surface that does not fluoresce, a clean Raman spectrum can be recorded.

2.3.3 Pure Water Scenario

Pure water produces one of the clearest examples of a Raman spectrum for a tri-atomic molecule. The deionized water spectrum in Figure 2.3 clearly shows the bond stretching and bending regions with O-H stretching defined between 2800 and 3800 cm^{-1} and the O-H bending region defined between 1500 and 1800 cm^{-1} [34]. As previously noted in Section 2.3.1, the stretching region incorporates both the symmetric and asymmetric stretching modes. The bending region is often neglected because it exhibits such a low Raman intensity that any fluorescence may obscure the signal in this region. The stretching mode of the water molecule creates strong Raman scattering and, therefore, most clearly shows any change to the water Raman spectrum when ions are present. For this reason, the stretching region of the water Raman spectrum will be the focus for the remainder of this analysis.

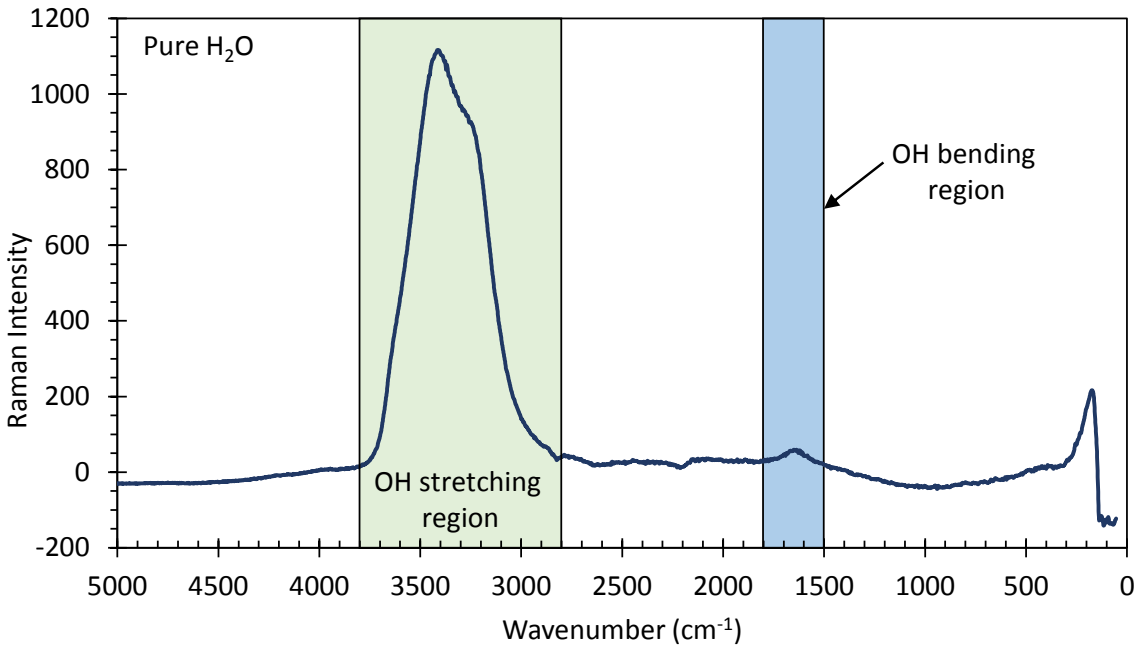

Figure 2.3: Raman spectrum for deionized water at 20 °C specifying the O-H stretching and bending regions.

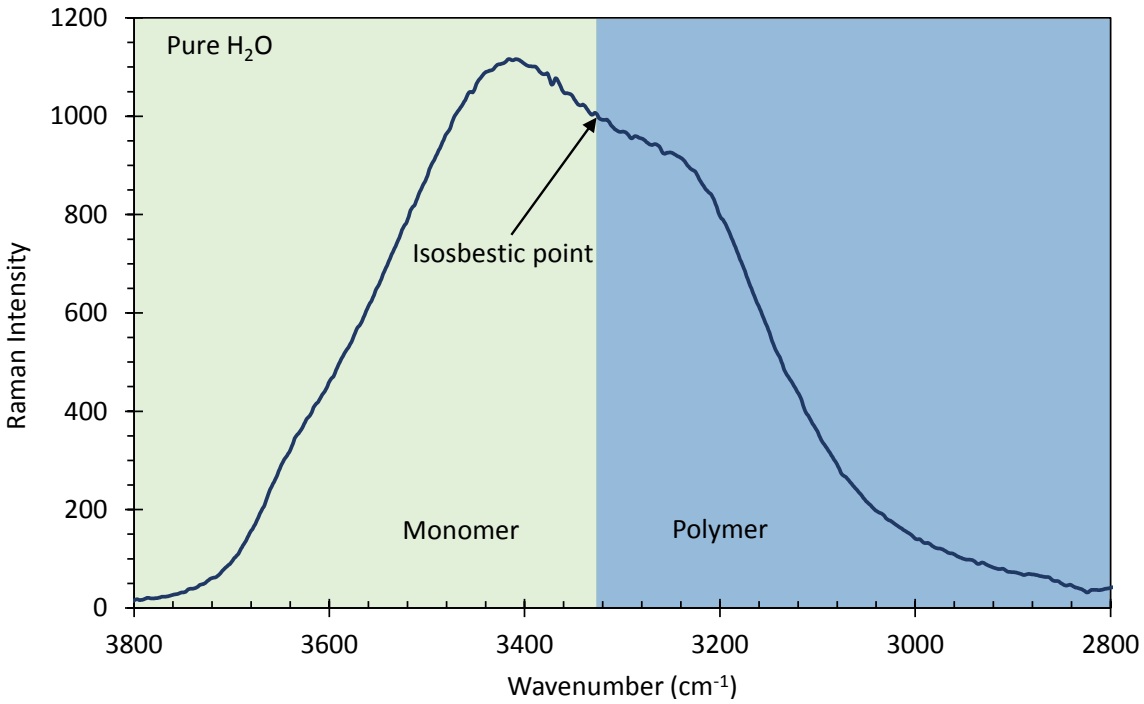

Figure 2.4: The O-H bond stretching region of the pure water Raman spectrum at 20 °C with the isosbestic point and the monomer and polymer regions defined.

The stretching region of the water Raman spectrum has key features that can be used to characterize the concentration of the water sample. Upon close inspection, the water stretching region can be divided into two main peak contributions, which superimpose into the peak depicted in Fig. 2.4. There are multiple theories as to what these peaks represent, but most agree that they hint at two states of water. The higher wavenumber peak (left in Fig. 2.4) is often called the monomer peak and represents the water molecules that are not hydrogen bonded to another molecule, while the lower wavenumber peak is called the polymer peak and represents the hydrogen bonded molecules [35]. As the temperature and concentration of the solution vary, the relative heights of the monomer and polymer peaks change as the water molecule intramolecular O-H bonds are formed and broken forming monomers and polymers [35, 36]. Between these two peaks is the isoskedastic point, or what

is also commonly called the isosbestic point [37]. The isosbestic point is defined as the wavenumber and Raman intensity at which all the Raman spectra for a given solution will intersect, regardless of concentration, as long as the chemical composition for the sample remains the same. While the isosbestic point is accepted as unchanging for samples with the same chemical composition, the actual location of the isosbestic point has been argued over the years because the location varies based on the polarization of the water molecules [37]. With this discovery, the accepted isosbestic point for salt solutions of liquid water lies in the range from 3325 to 3356 cm^{-1} [36, 38, 39]. Many analysis techniques discussed herein use the location of the isosbestic point and the monomer and polymer halves of the water Raman spectrum to determine the concentration of salt ions in a liquid water sample.

2.3.4 Established Methods for Determining Concentration with Raman Spectroscopy

Raman spectra can provide information about the concentration of ions within an aqueous solutions through a myriad of methods. Most existing methods are built on Gaussian deconvolution or a variation of a ratio of integrated key spectra areas.

Li and coworkers implemented Gaussian deconvolution on Raman spectra of aqueous solutions with $CaCl_2$ and $MgCl_2$ separately [40]. The Gaussian deconvolution was completed by parsing the stretching region of the water Raman spectrum into five Gaussian curves with the location of each center fixed at a specified wavenumber because the center locations of each contributing curve had been previously proven to not change with temperature. The Gaussian curves were then combined into a ratio by taking the area of the three highest wavenumber peaks and normalizing it by the whole integrated intensity for the water stretching region (2800 to 3800

cm^{-1}). This ratio was found to vary linearly with the solution concentration and can therefore be used to determine the concentration of the solution. Likewise, Pereira-Neto and coworkers analyzed aqueous solutions of lithium perchlorate with the use of Raman spectroscopy [38]. Unlike Li and coworkers, Pereira-Neto and coworkers performed a six Gaussian peak deconvolution with three peaks below the isosbestic point wavenumber and three peaks above the isosbestic point. The area of the lower wavenumber peak set was then divided by the area of the higher wavenumber peak set to create a ratio to determine concentration. While both Li and Pereira-Neto produced results that can be used to determine the concentration of a solution from a Raman spectrum, we found this peak fitting to be numerically intensive, with a minimum of 1,000 iterations of deconvolutions required to achieve a coefficient of determination of at least $r^2 = 0.99$ for the peak areas. This corresponds to about a computation time of about 30 minutes for each Raman spectrum that is collected and analyzed with a standard desktop computer using the general purpose Matlab tool.

To move away from time consuming Gaussian deconvolutions, Furić and coworkers worked with NaCl aqueous solutions and introduced the idea of subtracting a reference Raman spectrum from each collected Raman spectrum. The intensity of the adapted spectrum was recorded and normalized by the intensity of the reference spectrum to find a ratio that can be used to determine the concentration of the sample [41].

In an attempt to determine the concentration of aqueous salt solutions, regardless of the chemical makeup of the salt, a few researchers developed methods using a ratio of the areas of the Raman spectrum without incorporating Gaussian deconvolution. Georgiev and coworkers introduced the idea of the skewing parameter where the stretching region of the water Raman spectrum was divided into two equal halves with an arbitrary midpoint [42]. Then, each half was integrated and a ratio was created from the area of each half. This ratio was used to determine the concentration of the

solution. Though Georgiev and coworkers advertised that their skewing parameter can determine the concentration of salt in a solution as long as there is only one type of salt present, Mernagh and coworkers wanted to make the system work with a variety of chloride salt solutions with multiple salts in solution [39]. Therefore, Mernagh and coworkers built upon Georgiev and coworkers studies by introducing a cation correction factor. This correction factor was multiplied by the skewing parameter in a modified ratio calculation. Like, Georgiev and coworkers, Mernagh and coworkers chose arbitrary wavenumbers as points of interest in their calculations. Đuričković and coworkers took the skewing parameter calculations performed by both Georgiev and Mernagh and linked the boundary variable to significant points on the spectrum [36]. Instead of choosing an arbitrary number in the middle of the two main peaks for the water stretching region, Đuričković and coworkers used the isosbestic point, discussed in Section 2.3.3, as the midpoint. With a more rigorous and scientifically based midpoint, Đuričković and coworkers then used the same equal intervals that Georgiev and Mernagh used to determine the beginning and end to their peaks areas. While all these studies claim to work regardless of the salt in the aqueous solution, most have only been demonstrated for chloride salt solutions.

2.4 Summary

State and local transportation agencies spend a significant amount of resources annually to maintain safer winter driving conditions. In an effort to decrease their budgets and the environmental impact that their methods create, many transportation agencies are looking to determine the amount of salt on the roadway in real time. While there are a few methods for determining the salt concentration on the roadway, each method comes with its own advantages and disadvantages. Many of the preexisting

methods have difficulties sensing the presence of both chloride and acetate based salt deicers.

While Raman spectroscopy cannot directly sense the concentration of salt in a solution because the salt particles disassociate in the solution, this becomes an advantage when working with salt of varying chemical composition. Instead of looking directly at the salt particle, the Raman spectrum analysis methods monitor the changes in the water Raman spectra when a known salt is added; therefore, to know the concentration of salt in the solution, the way in which each salt changes the spectrum must be analyzed. Because of this and a few other advantages, we propose using Raman spectroscopy to determine the concentration of salt on the roadway. This thesis works toward optimizing the analysis methods to determine the concentration of a sample in near-real time and optimizing the material used as a testing platform to minimize the effects of fluorescence.

Chapter 3

Sample Characterization Methodology

The chosen sample preparation and data collection techniques employed throughout this study mimic the setup that a sample collected from the roadway is envisioned to be analyzed using a mobile Raman spectroscopy salinity sensor.

3.1 Experimental Setup

3.1.1 Sample Preparation

Throughout this study, all aqueous salt samples were made from anhydrous salts dissolved in deionized water. The NaCl, $CaCl_2$, $MgCl_2$, and KAc salts were purchased from Sigma Aldrich, while 96% pure commercial grade CMA was purchased from the Green Earth Deicing Company, Inc. Each sample was prepared at room temperature by measuring a specified mass of each salt and combining it with deionized water

to produce a targeted concentration. To verify the concentration of the samples, an inductively coupled plasma mass spectrometer (ICP-MS) was used for the chloride solutions and a conductivity probe for the acetate solutions.

The aqueous chloride and acetate salt samples used in this study were made at concentrations ranging from pure deionized water to a saturated mixture, making sure to include the eutectic concentration for each salt. However, this study only tested CMA salt solutions from pure deionized water to just below the eutectic concentration due to the amount of insoluble particles that were present in the sample at higher concentration. Each sample was thoroughly shaken at room temperature to ensure that all salt granules had dissolved. The samples were then shaken again immediately prior to testing to ensure that the solution was homogeneous. This ensured that the concentration of the tested sample was the same as the concentration of the parent solution.

3.1.2 Testing platform

This study used a testing platform designed to mimic real world data collection of aqueous samples by implementing technology that the final design will incorporate. The aqueous salt solution samples were prepared for analysis by first placing 0.6 mL volume of the solution in a 3 mm deep sample well milled into the top surface of an aluminum plate. The aluminum plate was bolted to the top of a thermoelectric cold plate cooler (TE Technology CP-200HT-TT) with the capability of reaching -20 °C at normal ambient room temperatures. The cold plate was temperature controlled via a proportional-integral-derivative controller (TE Technology TC-36-25-RS485) receiving the temperature readings from a 5 KΩ thermistor fixed to the plate (next to the sample well) without touching the sample (Fig. 3.1). Marine epoxy coated the exposed bead of the thermistor to protect it from contact with the sample or water

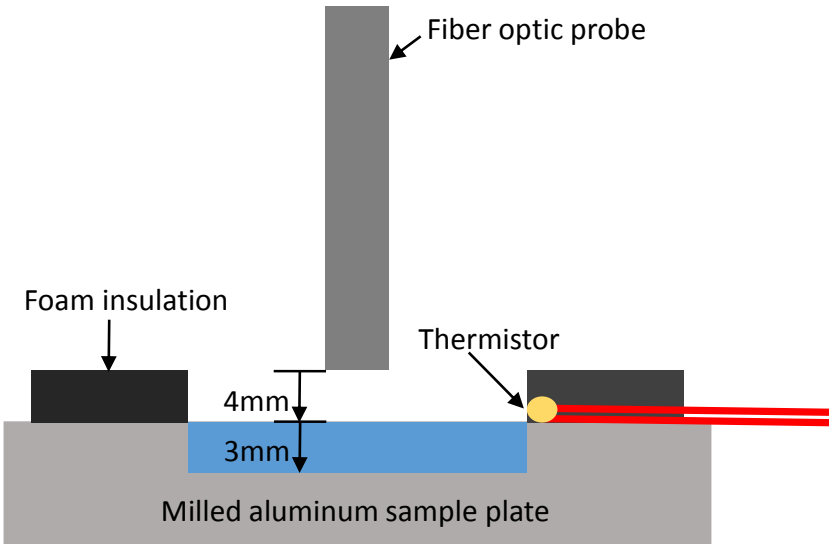

Figure 3.1: Pictorial representation of the fiber optic probe and thermistor arrangement used to gather the Raman spectra of each sample placed on the sample plate.

droplets forming as the ambient temperature decreased. To speed up the sample cooling, the cold plate and aluminum plate system were insulated to limit the thermal exposure to ambient air and increase the speed at which the system reached thermal equilibrium when the temperature was set.

The thermistor position added to the offset in the temperature reading for the sample because of its contact with the ambient air which was corrected after the samples were analyzed. This offset was characterized by placing the aluminum sample plate in an insulated bath of deionized ice water and recording the temperature with the thermistor and a thermocouple every 30 seconds over a 5 minute interval. The thermocouple read an average temperature value of -0.04 °C with a standard deviation of 0.05 °C, and the thermistor bonded to the plate read an average temperature of -2.15 °C with a standard deviation of less than 0.01 °C. The thermistor consistently read 2.11 °C less than the thermocouple which is used herein as the value of the offset. While the aqueous salt samples were tested from +20 to -20 °C, correcting for the offset changes the temperature range to +22 to -18 °C.

The Raman spectra were collected using a Thermo Scientific DXR Raman Microscope outfitted with an extended range grating that provided the spectrum values from 50 to 600 cm^{-1} with 11 cm^{-1} resolution. This study used an InPhotonics fiber optic probe to excite the sample with a 532 nm excitation wavelength light beam and collect the reflecting beam. To collect the reflecting beam, the fiber optic probe was orientated with an approximate focal distance of 4 mm with slight adjustments to achieve the largest signal Raman intensity (Fig. 3.2). The Raman spectrometer used the collected beam to create the Raman spectrum.

Figure 3.2: Fiber optic probe test setup for the sample characterization tests after removing the foam housing that was used to shield the setup from the ambient air. The focal distance between the fiber optic probe and the sample remained around 4 mm throughout all of the tests.

3.1.3 Contaminated Sample Scenario

Since the mobile Raman spectroscopy salinity sensor will collect the roadway samples via tire splash or read the samples off the roadway, sand particles are expected to appear in the sample. Therefore, characterizing changes in the Raman signal caused by the presence of sand is required to calculate solution concentrations accurately. A special NaCl sample was made to determine the Raman spectrum of a solution contaminated by sand. Following the FHWA's recipe for a 23% NaCl solution commonly used for anti-icing measures, a eutectic concentration solution was made based on the volume of water [17]. While the FHWA's formula was designed for commercial grade rock salt with a maximum of 5% impurities, the sample in this study was made using 99% pure anhydrous NaCl. This NaCl sample for the contaminated sample test is more concentrated than most DOTs make in-house, but it provides a good model for how the sand grains will affect the Raman spectrum when a sample is taken from the roadway.

NDOT's salt-sand pile provided the sand grains for this portion of the study. The salt-sand mixture was dissolved in deionized water to separate the sand particles. A filter then separated the sand grains from the liquid solution, and the resulting sand particles were rinsed with ethanol to ensure that only the sand grains remained. ICP-MS was used to characterize the ions in the strained liquid solution created by mixing the salt-sand mixture with deionized water. All of these steps were taken to fully understand the solution placed in the sample area prior to testing.

Prior to testing, a few sand grains were placed in the sample dimple milled into the aluminum plate. The FHWA NaCl salt solution then filled the sample area, making certain to not overfill the sample dimple (Fig. 3.3). With the contaminated sample setup complete, the test setup described in Section 3.1.2 was used to collected the Raman spectrum for the contaminated sample scenario.

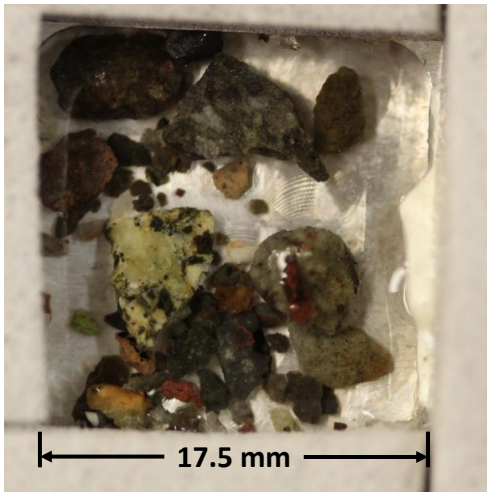

Figure 3.3: Contaminated sample formed by placing clean sand grains in the 17.5 mm by 17.5 mm square sample dimple and pouring the FHWA's NaCl deicing salt solution atop until the dimple in the sample plate was filled.

3.2 Data Collection

The Raman spectra for each salt solution was collected over a variety of temperatures and concentrations using a Thermo Scientific DXR Raman Microscope with a fiber optic probe. The Raman spectrometer was set to record 12 measurements, each with a 5 second sampling time. The machine averaged the measurements to create the Raman spectra for the sample at the specified temperature and concentration. The Raman spectrum was collected a minimum of three times to ensure that the sample had reached thermal equilibrium with the cooling system before moving to the next lower temperature. After correcting for the thermistor bias, samples were tested from 22 to -18 °C starting at 22 °C and working down in temperature until the sample reached its liquidus or until -18 °C was reached. Every sample was tested at 5 °C increments from 22 to 7 °C. The NaCl solutions were then tested from 6 °C until the -18 °C or until the liquidus was reached at 2 °C increments while the remaining solutions were tested at 4 °C increments. The NaCl solutions experienced higher resolution tests because there is more published data to compare with for NaCl

solutions while the remaining salt solutions are quite new to concentration analysis. After subjecting each sample to measurements over a range of temperatures, the aluminum sample plate was rinsed with deionized water, dried, and filled with another salt solution and/or concentration.

3.3 Data Analysis

The data analysis techniques used throughout this study are based upon previously published Raman spectra analyses designed to work well with chloride salt solutions [36, 39, 42]. This study optimized and altered existing analyses to provide more consistent concentration readings for five of the most common salt deicers. The analyses were performed with the collected Raman spectra and the Raman spectra normalized to the isosbestic point. This provided an opportunity to assess whether the analyses would yield the same result regardless of how the data was processed before calculating the concentration. Removing unnecessary data manipulation accelerates the calculations so they provide results in near-real time.

3.3.1 Ratio of the Areas

The ratio of key spectral integrated areas, or ratio of areas, R_A, analysis has been applied by multiple research groups to determine the concentration of salt in an aqueous solution using the collected Raman spectra [36, 39, 42]. The R_A incorporated dividing the stretching region of the water Raman spectrum into two halves. The two regions are then integrated, and the area of the higher wavenumber halve is divided by the area of the lower wavenumber half. This ratio is then used to characterize the concentration of salt in a solution by comparing it to previously recorded ratios with the same chemical makeup.

The majority of published studies using the R_A analysis techniques apply equal integration intervals around a specified midpoint. The midpoint can either be an arbitrary value between the polymer and monomer peaks (Fig. 2.4) [39], or some researchers have elected to use the isosbestic point of liquid water as the midpoint [36]. The previously published studies have demonstrated that the calculations work consistently for aqueous chloride salt solutions, but additional salt solutions have only been briefly covered.

This study implemented the R_A analysis techniques for aqueous solutions of chloride and acetate salt solutions. The fiber optic probe's focal distance was adjusted for each sample to ensure that the maximum Raman signal was collected. Because the collected Raman spectra have varying maximum peak intensity values, it can be difficult to ascertain the exact isosbestic point location for the samples used. To easily compare the collected data, the midpoint value used in this study was fixed to 3325 cm^{-1}, the isosbestic value for aqueous water solutions that Đuričković and coworkers found [36]. The R_A calculations were then performed with equal and unequal integration integrals using

$$R_A = \frac{\sum_{3326}^{w_h} \left(\frac{I(i)+I(i-1)}{2} \times [i-(i-1)] \right)}{\sum_{3325}^{w_l} \left(\frac{I(i)+I(i-1)}{2} \times [i-(i-1)] \right)} \tag{3.1}$$

where w_h and w_l correspond to the wavenumber integration limits greater than and less than the isosbestic wavenumber respectively and I is the Raman intensity value corresponding to the wavenumber that the summation is currently considering. With each variation, the midpoint remained at 3325 cm^{-1} and the area of the higher wavenumber or monomer peak half of the water stretching region was divided by the area of the lower wavenumber or polymer peak half of the water stretching region (Fig. 3.4).

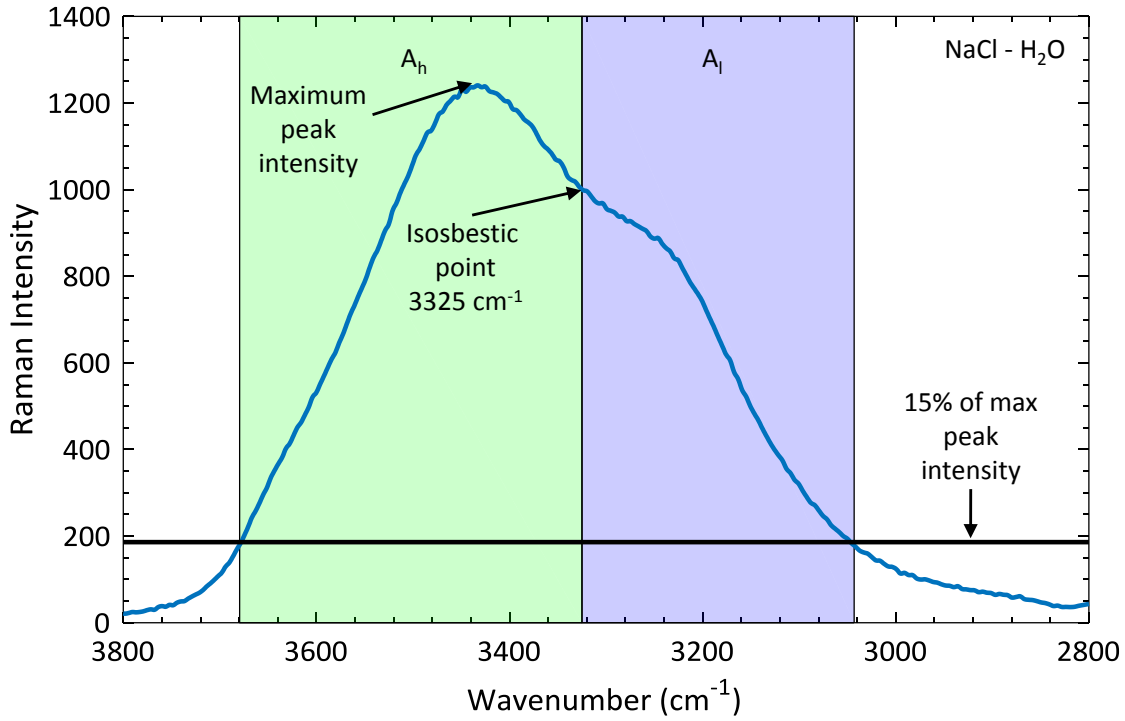

Figure 3.4: Raman spectrum of a 58 g/L NaCl solution with the high and low wavenumber areas partitioned using 15% of the max intensity and the isosbestic points as the limits of integration.

After performing multiple analysis iterations with equal and unequal integration intervals, this study found that more consistent R_A values were calculated with the start and end integration limits set to 15% of the maximum Raman peak intensity (Fig. 3.4).

After the R_A calculations are performed to characterize the collected Raman spectrum with a scalar value, benchmark plots showing how R_A wavies with tempearture and concentration for various salts can be created. Results from previous studies showed that R_A calculations work well for aqueous chloride salt solutions [36, 42], but DOT's across the country use both chloride and acetate salts to reduce the melting point of ice on a roadway. While some studies have proposed applying the R_A calculations to determine the concentration of acetate salt solutions [36], this study found

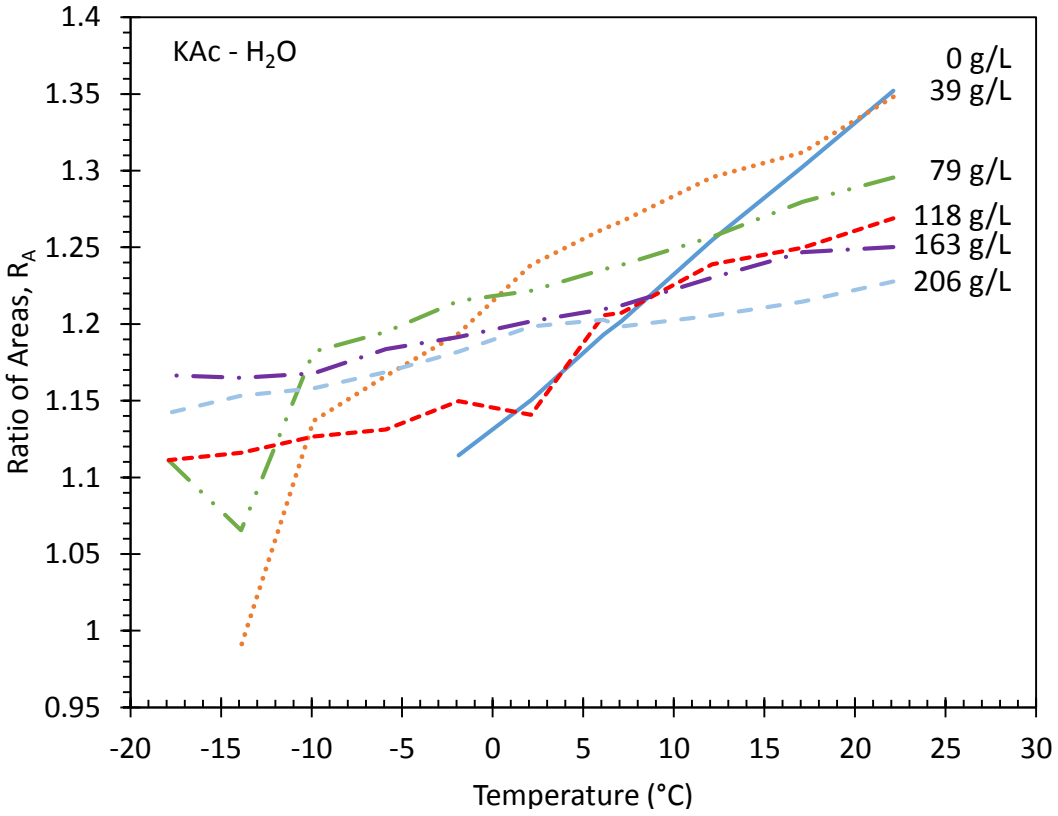

Figure 3.5: Benchmark plot resulting from R_A calculations performed on KAc solutions over varying concentrations and temperatures without removing the acetate peak influence. This shows that applying R_A calculations to the non-normalized Raman spectra for the acetate solutions produces non-meaningful benchmark plots.

that no clear trend is present for the R_A value when the calculations are performed on the non-normalized collected Raman spectra for aqueous acetate samples (Fig. 3.5).

To make the R_A calculations present clear trends on the benchmark plot for acetate solutions, the R_A calculations must include a separate calculation to remove the acetate ion contribution from the Raman spectrum. The following sections will detail how the combination of R_A calculations and Gaussian deconvolution can yield clear trends on the benchmark plots for acetate solutions.

3.3.2 Gaussian Deconvolution

Many previous studies used Gaussian deconvolution to determine the concentration of salt in a solution [38, 40]. Throughout these studies, anywhere from two to six peaks have been used to characterize the stretching region of the water Raman spectrum with pure water or water with chloride salts dissolved in the solution [35, 38, 43–46]. The Gaussian peaks were then used in additional calculations to determine the concentration of the aqueous solution. While previous studies have determined the concentration of salt in a solution via Gaussian deconvolution, most do not comment on how long their calculations take to perform or what resources or computational power were used to perform the calculations.

In this study, a Gaussian deconvolution tool developed by O'Haver was implemented to perform the Gaussian deconvolutions on the collected Raman spectra [47]. Only the stretching region (2800 to 3800 cm^{-1}) of the water Raman spectrum was subjected to Gaussian deconvolutions since it is the region of interest, and decreasing the data points submitted to the tool decreases the required computing time. While a Gaussian deconvolution with two peaks can capture the main monomer and polymer peaks [35], this study used five Gaussian peaks for chloride salt solutions and six for acetate salt solutions to get a coefficient of determination of at least, $r^2 = 0.99$. A minimum of 1,000 iterations were required to reach the desired coefficient of determination. Figure 3.6 demonstrates the results of the Gaussian deconvolution of a 39 g/L KAc solution at 20 °C with six Gaussian peaks and 1,000 iterations.

A fully unconstrained Gaussian deconvolution of the water stretching region with six peaks and 1,000 iterations takes up to 45 minutes to complete on a standard desktop computer. Fixing the center locations of the six Gaussian peaks during the deconvolutions reduces the computation time to as low as 10 minutes when performed on a standard computer with the general purpose Matlab tool [47]. To decrease the

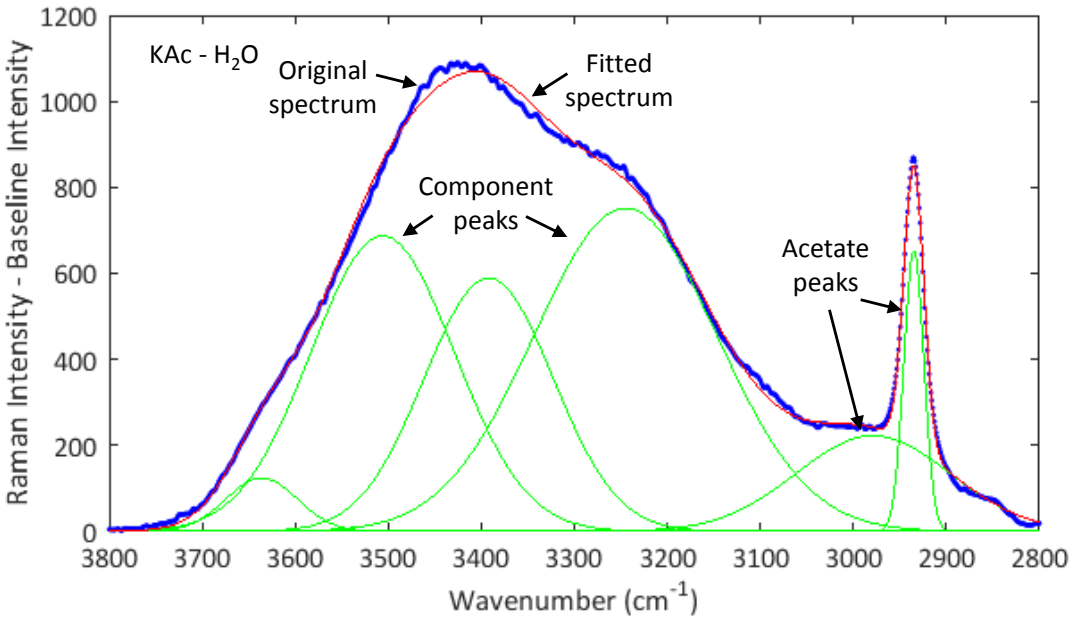

Figure 3.6: Raman spectrum of a 39 g/L solution of potassium acetate at 20 °C after subtracting the baseline equation and performing a Gaussian deconvolution with six component peaks.

calculation time further, the sample inputted into the Gaussian deconvolution tool can be reduced to only include the acetate peak contributions (2800 to about 3200 cm^{-1}). Applying the Gaussian deconvolution tool to the acetate contribution area of the spectrum will take less time and possibly require less iterations to complete the fit. With the two acetate peaks' contributions removed, the R_A calculations can be combined with the Gaussian deconvolutions to characterize the concentration of salt in a solution. Additionally, using a Gaussian deconvolution tool optimized to perform a regression with 15 parameters can possibly reduce the calculation time beyond that which was capable with a general purpose Matlab tool.

3.3.3 Gaussian Deconvolution and Ratio of the Areas

The concentration of aqueous acetate solutions cannot be consistently determined using R_A calculations alone and a time-consuming full Gaussian deconvolution of the entire stretching region of the aqueous solutions cannot produce concentration data in near-real time. To determine the concentration of acetate deicer solutions on the roadway, this study proposes a combination of R_A and Gaussian deconvolution to maintain the benefits of each method while consistently determining the concentration of a solution in near-real time.

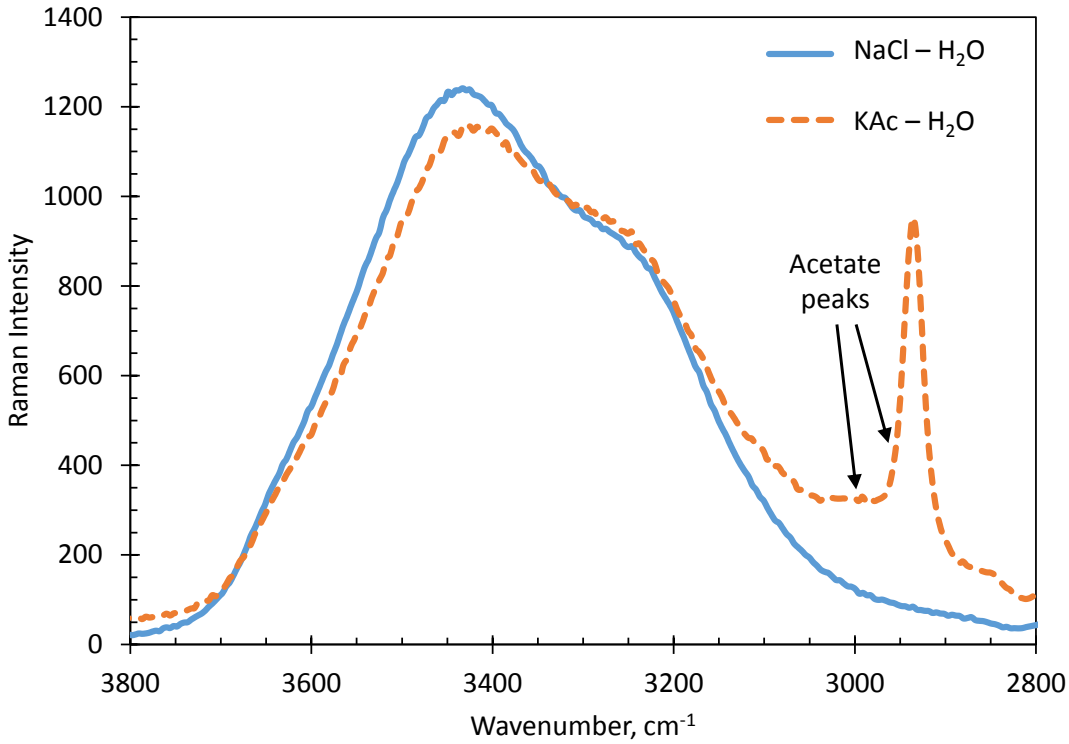

Figure 3.7: Comparison of the stretching region a 58 g/L NaCl solution and a 39 g/L KAc solution with both at 20 °C showing the effect that the acetate peaks have on the area of the polymer peak.

In order to implement the R_A calculations with consistent results for acetate solutions, a Gaussian deconvolution was first performed to remove the acetate peaks' influence and return the stretching region of the water Raman spectrum to its char-

acteristic shape seen with chloride salt solutions (Fig. 3.7). While performing the Gaussian deconvolution on just the acetate peak contributions to the stretching region of the water Raman spectrum would speed up the fitting process, this study performed the deconvolutions on the entire stretching region in order to record a good coefficient of determination. The peak center locations for all six peaks were fixed throughout the Gaussian deconvolutions to speed up the calculation process: 2935, 2978.89, 3245, 3392, 3506, and 3636 cm^{-1}. The peak values were chosen based off of the values reported by Carey and coworkers for the water contribution and by performing a series of Gaussian deconvolutions on the entire stretching region [46]. The acetate peaks varied only slightly, so the mean peak values were used. Because the Gaussian deconvolution tool [47] could provide inconsistent results at 1,000 iterations, the width of the higher wavenumber acetate peak (2789.89 cm^{-1}) was held constant at 184 cm^{-1} to ensure that the acetate contributions were subtracted consistently. With the center locations and width held constant, the Gaussian deconvolution provided the peak height and full width at half maximum (FWHM) value needed to remove the acetate peaks' contributions to the stretching region.

Using the acetate peaks' center locations, heights, and FWHM values, a general purpose Matlab code was used to subtract the Gaussian peaks from the non-normalized aqueous acetate solution spectra. Removing the acetate peaks creates an adjusted spectrum (Fig. 3.8) is similar in shape to the stretching region shape created by the chloride solutions. The R_A calculations were then performed on this adjusted spectrum, as detailed in Section 3.3.1. The combination of Gaussian deconvolution and R_A calculations is slower than the R_A calculations alone, but the combination is necessary to find consistent concentration results from the collected acetate solution Raman spectra. Because the Gaussian deconvolution of the stretching region took a minimum of 10 minutes the the general purpose Matlab tool [47] and the R_A calcu-

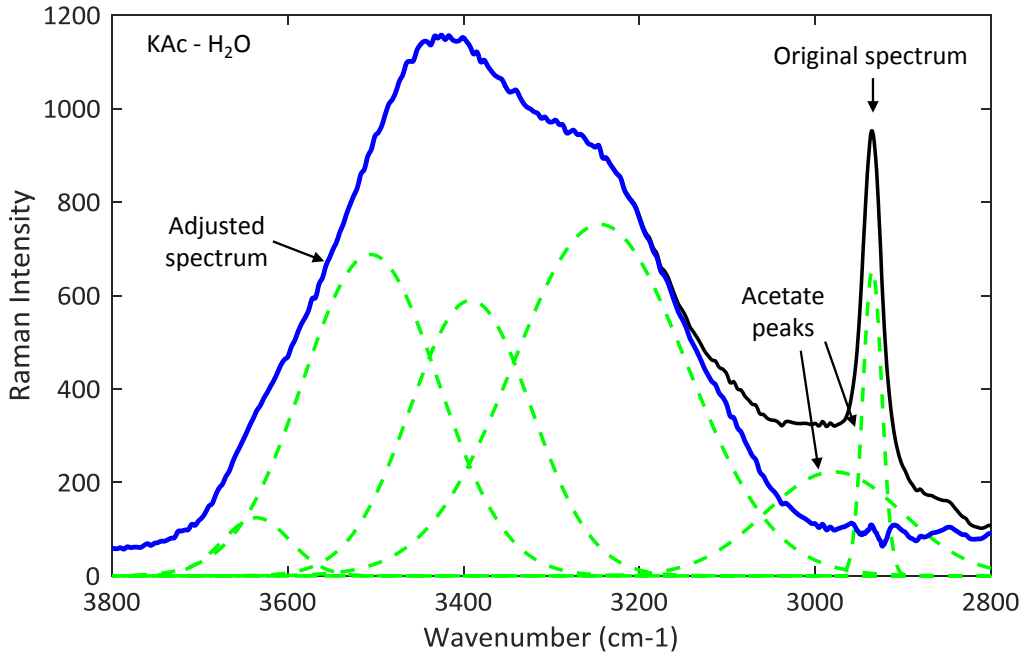

Figure 3.8: Stretching region of the water Raman spectrum for a 39 g/L solution of KAc at 20 °C with the adjusted spectrum representing the stretching region with the acetate peaks' influence removed.

lations take seconds, a more optimized Gaussian deconvolution program would need to be used to report the concentration of acetate solutions in near-real time.

3.4 Summary

In order to demonstrate that Raman spectroscopy can determine the concentration of aqueous solutions containing one of the five most common salt deicers, samples were created for each salt over a range of concentrations, including the eutectic concentration. Each sample was then tested from +22 °C to -18 °C,or until the liquidus point had been reached. A Thermo Scientific DXR Raman Microscope, fiber optic probe, and 532 nm excitation laser were used to collect the Raman spectrum of each sample at each temperature step.

Once the Raman spectra were collected, each sample was subjected to R_A calculations to determine the concentration of the sample at a given temperature. As with previously published studies, the R_A calculations were able to determine the concentration of the chloride salt solutions by taking the ratio of the areas on either side of the isosbestic point of the collected Raman spectra. The R_A calculations can be performed on a set of Raman spectra in a few seconds (near-real time). The acetate salt solutions required the use of Gaussian deconvolution to remove the effects of the acetate ions from the stretching region of the water Raman spectrum before the R_A calculations yielded meaningful results. Using a general purpose Matlab code and a standard desktop computer, the Gaussian deconvolution-based peak subtraction can be performed in as low as 10 minutes, but it is possible that the calculation can be performed in near-real time with a regression program designed to work with 15 parameters. Through multiple iterations of calculations, it was determined that using integration start and end points that corresponded to 15% of the maximum peak intensity yielded the most consistent concentration value results. Upon completing the R_A calculations, benchmark plots can be created relating the R_A scalar value, the sample concentration, and sample temperature for each of the five most common salt deicers. These results will be presented in Section 5.

Chapter 4

Surface Characterization Methodology

Throughout this study, the concentrations of various aqueous salt solutions were determined from their Raman spectra, collected when the samples were placed on a milled aluminum plate; however, the final design of the mobile salinity sensors using Raman spectroscopy will most likely use a stainless steel plate as the surface. To determine whether a change in the testing surface would change the calculated concentration values or the fluorescence in the Raman spectrum, various tests were performed with deionized water on 410 stainless steel surfaces with various surface preparation techniques and surface orientations.

4.1 Surface Preparation

The 410 stainless steel samples were subjected to two different surface treatments: unidirectional and non-directional surface finishing. The unidirectional sawn surface

finishing resulted from cutting the stainless steel disk samples from a rod. Using an optical profilometer housed inside an RTec Universal Tribometer, it was determined that the average surface roughness (R_a) for the as-cut sawn specimen was 0.91 μm. The two non-directional surface finishes were created by first sanding both samples with 120 Grit sandpaper by hand using a lapping machine until the unidirectional grooves were no longer present and the average roughness was about 0.14 μm. One of the disks was then subjected to 240 Grit sandpaper which further reduced it average surface roughness to 0.07 μm. After the surface of each of the three 410 stainless steel disks was finished, each was ultrasonically cleaned in deionized water with an iSonic P4800 ultrasonic cleaner for 180 seconds. Upon completion, each sample was removed, rinsed with ethanol, dried with a lint free cloth, and wrapped in a clean cloth until the sample was ready for testing.

4.2 Test Setup

Each surface test was completed by collecting the Raman spectrum of a deionized water sample sprayed on each surface over a variety of surface orientations using the Raman spectrometer setup described in Section 3.1.2. The samples were tested with the surface lying horizontal on the cold plate and inclined at a 30° angle relative to the cold plate. The 30° angle was chosen to characterize the difference in the Raman spectrum for a symmetric and an asymmetric droplet shape while allowing the probe to collect the spectra with the probe's long axis perpendicular to the cold plate. Each water droplet tested ranged in diameter from 2 to 4 mm (Fig. 4.1). The height of the water droplets was analyzed via a goniometer with the stage parallel to the ground and incline at a 30 ° angle. Using a block with a height of 3.13 mm as a reference, the maximum height of the water droplets was determined to be about 2.22 mm (Fig.

4.2). This is in stark contrast with the 3 mm deep samples used to characterize the sample concentration in Chapter 3. The water droplets were sprayed on the surface in a horizontal position until the water droplet reached the desired diameter. Each surface was then tested in three different orientations at 5 °C , using with same cold plate setup as was used for the sample characterization tests (Section 3.1.2).

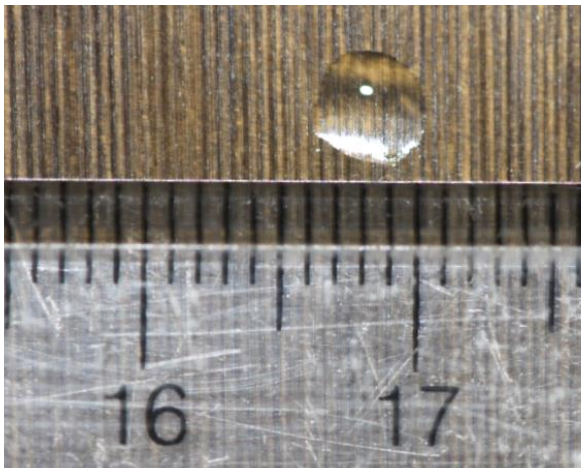

Figure 4.1: Magnified view of the average sized deionized water droplet showing a diameter of about 4 mm on the as-cut sawn sample surface.

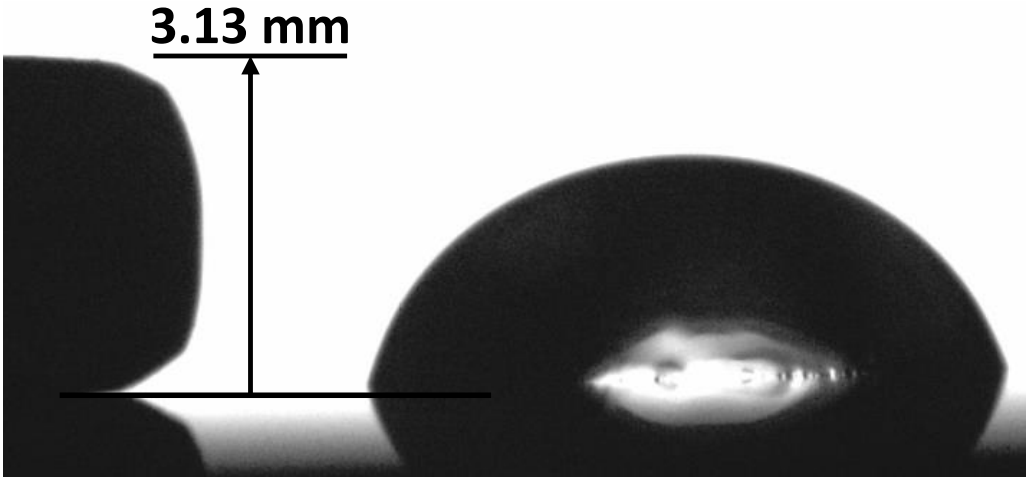

Figure 4.2: Average water droplet sprayed onto the surface with the maximum droplet height determined by comparing it to a block with a height of 3.13 mm and recorded with the sample stage parallel to the ground.

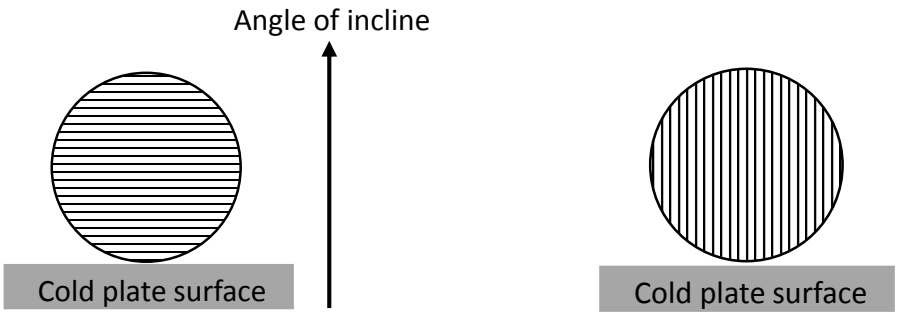

(a) (b)

Figure 4.3: Orientation of the as-cut sawn surface with the grooves (a) perpendicular to the incline and (b) parallel to the incline.

Each 410 stainless steel sample was first tested with the surface lying horizontal on the cold plate and the long axis of the fiber optic probe oriented perpendicularly to the surface. The fiber optic probe was fixed with a focal distance of 4 ± 0.5 mm, with slight adjustments to maximize the Raman intensity of the collected spectra. After the surface had reached 5 °C and the Raman spectrum was collected for the horizontal surface, the surface was inclined at a 30° angle with the use of a 3D printed holder. For the as-cut sawn samples, test were performed separately with the grooves perpendicular (Fig. 4.3a) and parallel (Fig. 4.3b) to the incline. In this orientation, the fiber optic probe was first oriented perpendicular to the cold plate when the Raman spectrum was collected (Fig. 4.4a). This ensured that the laser impinged upon the water droplet with a 30° angle. Lastly, the Raman spectrum was collected with the fiber optic probe perpendicular to the testing surface while the focal distance adjusted slightly to ensure the maximum Raman intensity signal was collected (Fig. 4.4b).

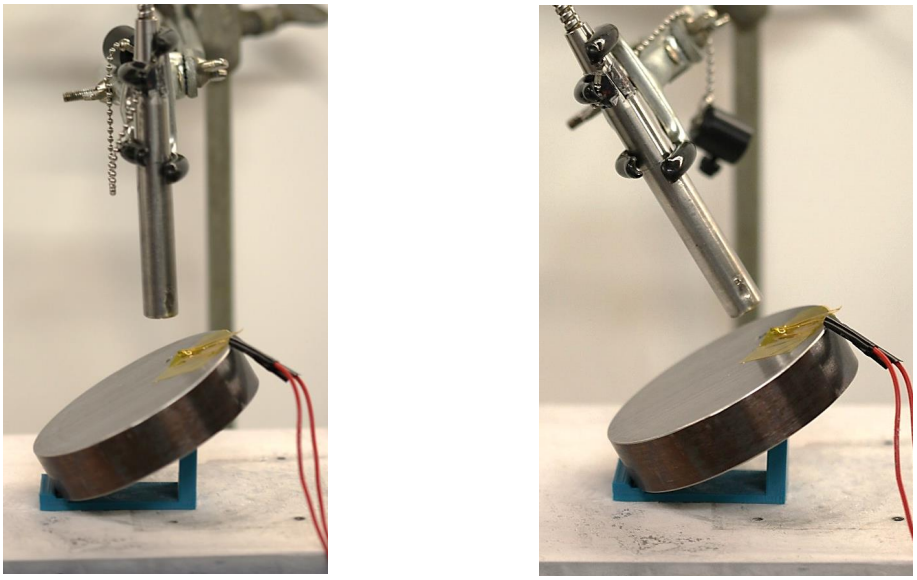

(a) (b)

Figure 4.4: Image of the sample surface inclined 30° from the cold plate surface with the fiber optic probe (a) perpendicular to the cold plate surface and (b) perpendicular to the testing surface.

4.3 Data Analysis

The Raman spectra collected for the various surface treatments and orientations were subjected to R_A calculations to determine if the surface preparation affected the calculations concentration for the sample. Gaussian deconvolution-based peak subtraction was not used because deionized water was the tested sample which does not have an additional peak in the water stretching region. Because any effect on the calculated concentration would be caused by fluorescence of the fiber optic probe interfering and altering the relative height of the monomer and polymer peaks, fluorescence of the signal was recorded prior to applying the R_A calculations. The R_A calculations were applied according to the method used for the sample characterization tests (Section 3.3.1). After calculating the R_A for each surface treatment and orientation, the scalar values were compared to the data at 5 °C on the chloride solution benchmark plots.

4.4 Summary

To determine the effect of the substrate surface on the gathered Raman spectrum, three 410 stainless steel samples were subjected to different surface treatments. Two samples were subjected to sanding which results in a non-directional surface finish while the third had unidirectional sawn surface grooves created when the sample was partitioned using a band saw. Each sample was then cleaned and subjected to Raman spectroscopy with a deionized water sample as the test subject. The test setup was the same as that used in the sample characterization section so that the results could be easily compared. The resulting Raman spectrum was subjected to R_A calculations and compared to the benchmark plots of the chloride solutions to determine if the change in testing surface would change the calculated concentration of the sample. The results are provided in Chapter 5.

Chapter 5

Experimental Results

The Raman spectra for the five most common chloride and acetate salt deicers were collected from each sample on a milled aluminum sample plate over a range of temperatures and concentrations. The R_A values were then combined into benchmark plots relating the ratio value to the temperature and concentration for each salt deicer. Using these benchmark plots, the effect of sand particles and the testing surface on the concentration calculations could be determined. The following sections reveal the benchmark plots created through the R_A calculations performed with and without Gaussian deconvolution-based peak subtraction and the effect of sand and surface preparation on the Raman spectra.

5.1 Chloride Solutions

Throughout this study, calculations were performed on both the non-normalized Raman spectra and Raman spectra normalized to an isosbestic value of 1,000 Raman intensity collected for each salt over a range of temperature and concentrations. To validate the results of this study, a NaCl solution was made with a 120 g/L concentra-

tion and the collected Raman spectra over a range of temperatures were normalized. The spectra were then subjected to equal integration interval R_A calculations with the midpoint and integration limits set to the same values previously employed by Đuričković and coworkers in their published report [36]. The numerical integration was performed with subintervals one wavenumber in length to match those used by Đuričković and coworkers' [36]. The R_A results for the normalized spectra were then compared to Đuričković and coworkers' over a range of temperatures in Figure 5.1 to determine the accuracy of our solutions and implementation of the R_A calculations.

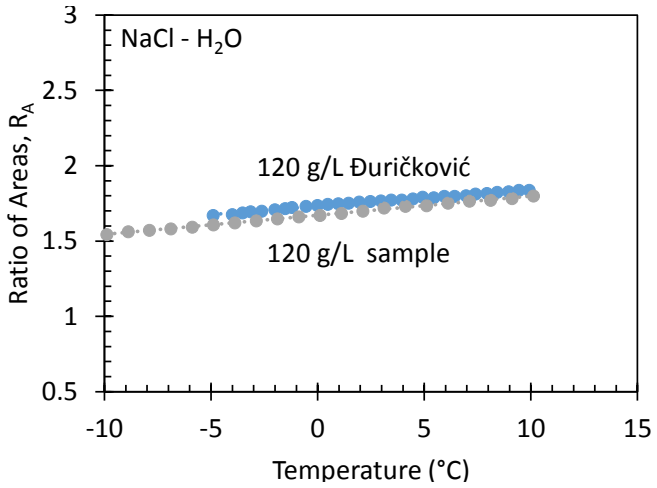

Figure 5.1: Benchmark plot comparison of our 120g/L solution subjected to equal integration interval R_A calculations compared to Đuričković and coworkers' published 120 g/L solution data with a maximum of a 4% difference [36].

The benchmark plot comparison depicts Đuričković and coworkers' data [36] with a trendline equation of $y = 0.011x + 1.731$ and our 120 g/L sample with a trendline equation of $y = 0.013x + 1.671$. The y-intercept difference implies that our 120 g/L solution is less concentrated than Đuričković and coworkers'; however, at most, there is a 4% difference which is within their reported accuracy (5%) [36]. Because the sample concentration was verified with the use of a conductivity probe, mass calculations, and an ICP-MS machine, and the trends relating the R_A values to sample

temperature are consistent between the previously published data and our data, the analysis method was considered valid.

Following the validation of our sample concentrations with the 120 g/L NaCl solution, the Raman spectra were collected for the remaining chloride salts and concentrations. The collected Raman spectra were then normalized, and the non-normalized and normalized spectra were subjected to R_A calculations to determine the relationship between the R_A scalar value, sample temperature, and sample concentration for each chloride salt. The chloride salt benchmark plots were created by mapping each R_A value to the corresponding temperature and concentration. From the created benchmark plots, the concentration of an unknown sample can be determined as long as the temperature of the sample is known.

5.1.1 Chloride Benchmark plots

As in most published studies, the benchmark plots created in this study were plotted showing the R_A scalar values versus sample temperature over a range of concentrations. The NaCl benchmark plots were created with the non-normalized and normalized Raman spectra and are shown in Figures 5.2 and 5.3 respectively. The benchmark plots show that the non-normalized and normalized Raman spectra experience the same trends in the R_A value as the concentration and temperature are varied, but a slight offset exists. The NaCl solutions experience an average difference of 0.5% between the non-normalized and normalized Raman spectra R_A values. Throughout the NaCl calculations, the normalized Raman spectra R_A calculations returned a lower concentration scalar value than the non-normalized Raman spectra when compared directly. This does not mean that one is more accurate than the other, but it does show that the R_A data processing procedure used for an unknown sample matches that used to make the benchmark plots to find an accurate concentration value.

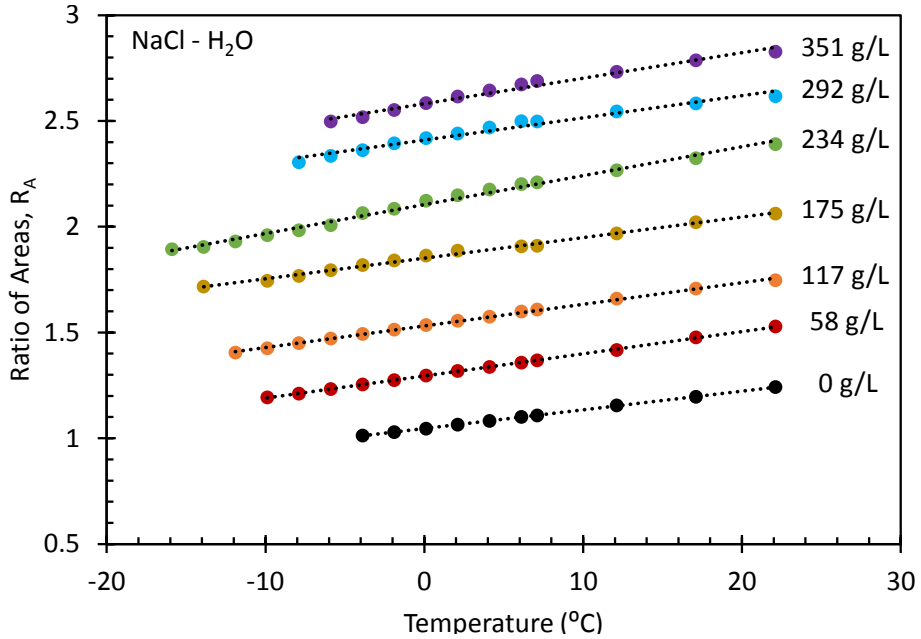

Figure 5.2: Benchmark plot created from the non-normalized Raman spectra of NaCl solutions over a range of concentrations and temperatures.

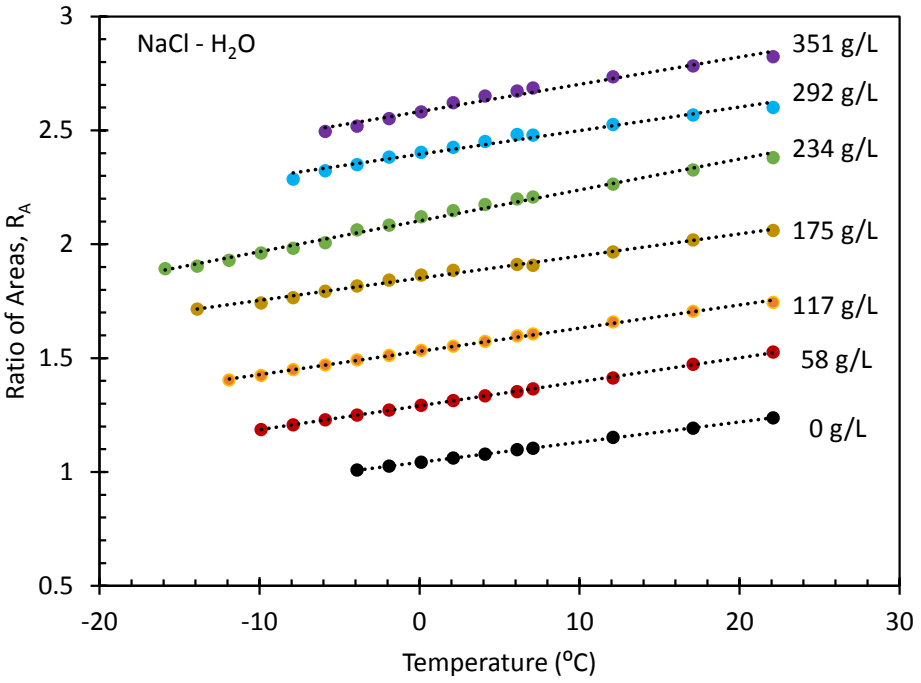

Figure 5.3: Benchmark plot created from the normalized Raman spectra of NaCl solutions over a range of temperatures and concentrations.

While the majority of published papers present their benchmark plots with the R_A scalar values plotted versus sample temperature, an alternate form of the benchmark plot compares the R_A scalar values to the concentration of the salt solution over a range of temperatures (Fig. 5.4). The alternative benchmark plot is easier to navigate with the naked eye. The concentration of an unknown sample can be determined after calculating the R_A scalar value and comparing it to the temperature line on the alternate benchmark plot for the corresponding salt. The alternate benchmark plot is more intuitive to navigate compared to the traditional, although the computer is able to navigate either with ease.

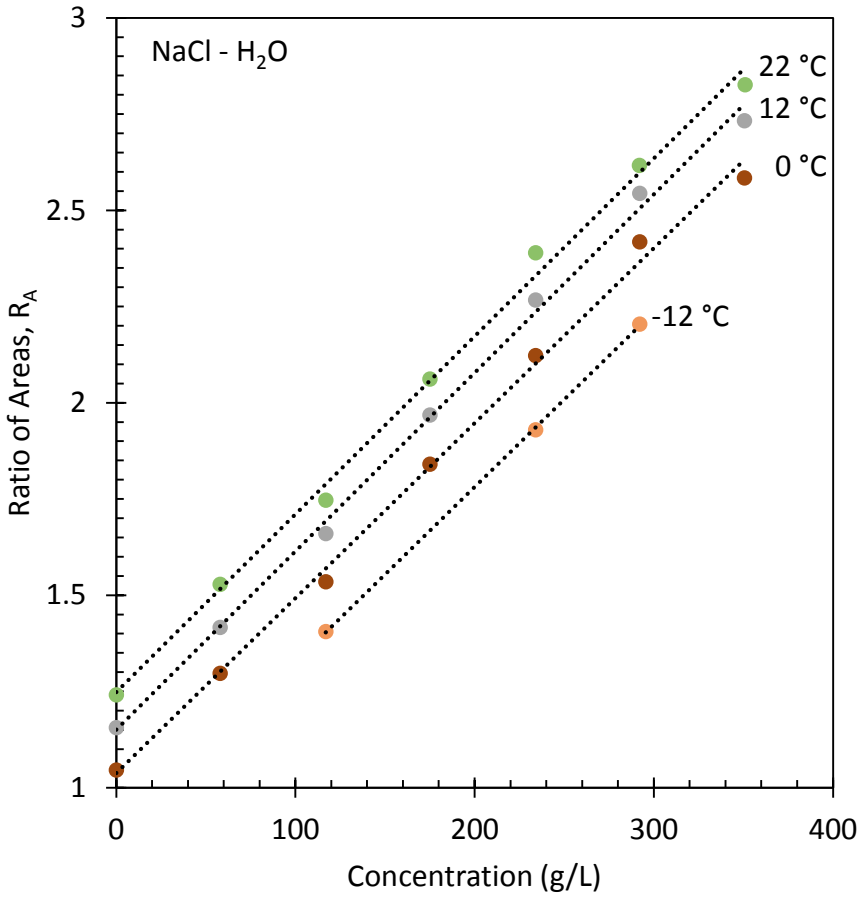

Figure 5.4: Alternative benchmark plot created using non-normalized Raman spectra from NaCl solutions with a few temperature shown.

The alternate form of the benchmark plot is created in the same way as the traditional benchmark plot; however, more concentrations are required for each deicing salt to clearly define the relationship between the R_A scalar value and the concentration of the sample over a range of temperatures. Additionally, the temperature line plots become clustered as tests are performed at more temperatures. To make the trendlines discernable, four temperatures with even spacing were plotted in Figure 5.4. In conclusion, while the alternate benchmark plot form facilitates estimating the concentration of an unknown sample when the salt and sample temperature are known, the traditional benchmark plot requires fewer concentrations to generate the trendlines.

For the remaining deicing salts tested throughout this thesis, the traditional benchmark plot comparing R_A scalar values to the sample temperature is used to present the data. The $CaCl_2$ benchmark plots created using the non-normalized and the normalized Raman spectra are shown in Figures 5.5 and 5.6 respectively. The $MgCl_2$ benchmark plots created using the non-normalized and the normalized Raman spectra are presented in Figures 5.7 and 5.8.

The $CaCl_2$ and $MgCl_2$ benchmark plots were made using the R_A calculations with unequal intervals and no peak subtraction. Like the NaCl benchmark plots, the $CaCl_2$ and $MgCl_2$ benchmark plots have a slight offset between the plots created from the non-normalized and normalized Raman spectra that can only be identified by closely comparing the data points from each plot. Both the $CaCl_2$ and $MgCl_2$ benchmark plots experience as much as a 2% difference between the non-normalized and normalized data. While this is larger than the percent difference found for the NaCl solutions, the difference does not affect the calculated concentration value as long as the same data processing procedure is applied to both the benchmark plot data and the unknown sample.

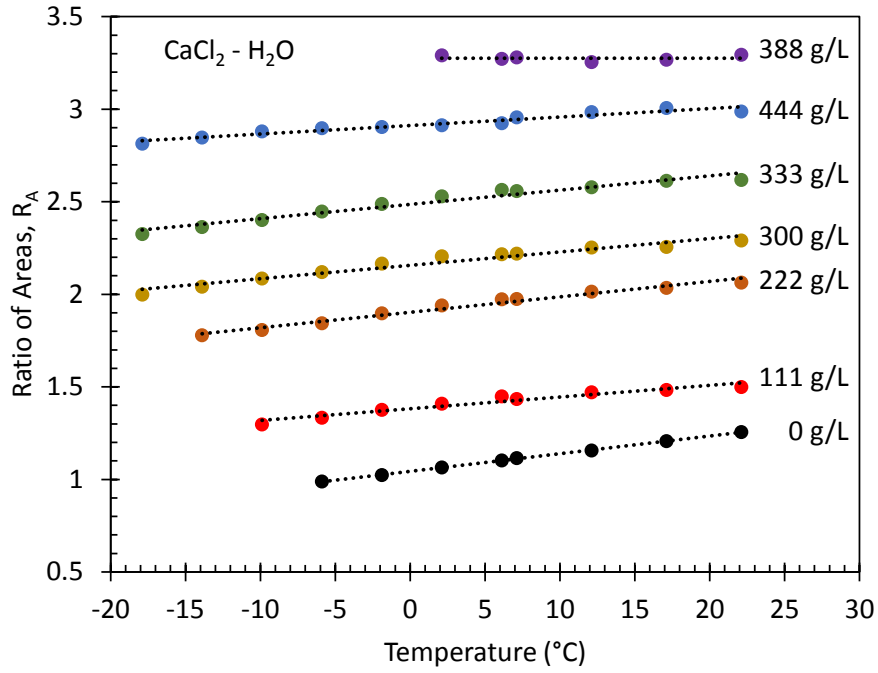

Figure 5.5: Benchmark plot created from the non-normalized Raman spectra of $CaCl_2$ solutions over a range of temperatures and concentrations.

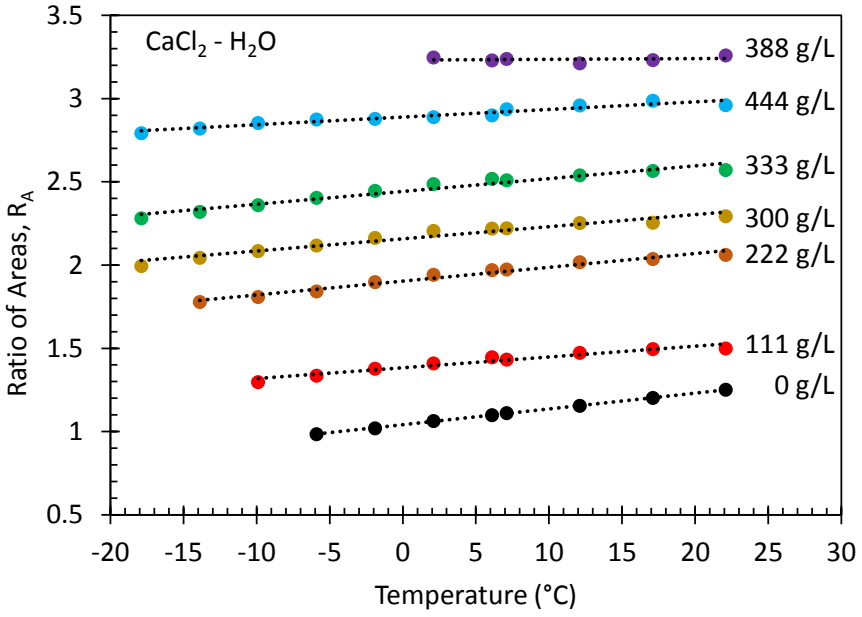

Figure 5.6: Benchmark plot created from the normalized Raman spectra of $CaCl_2$ solutions over a range of temperatures and concentrations.

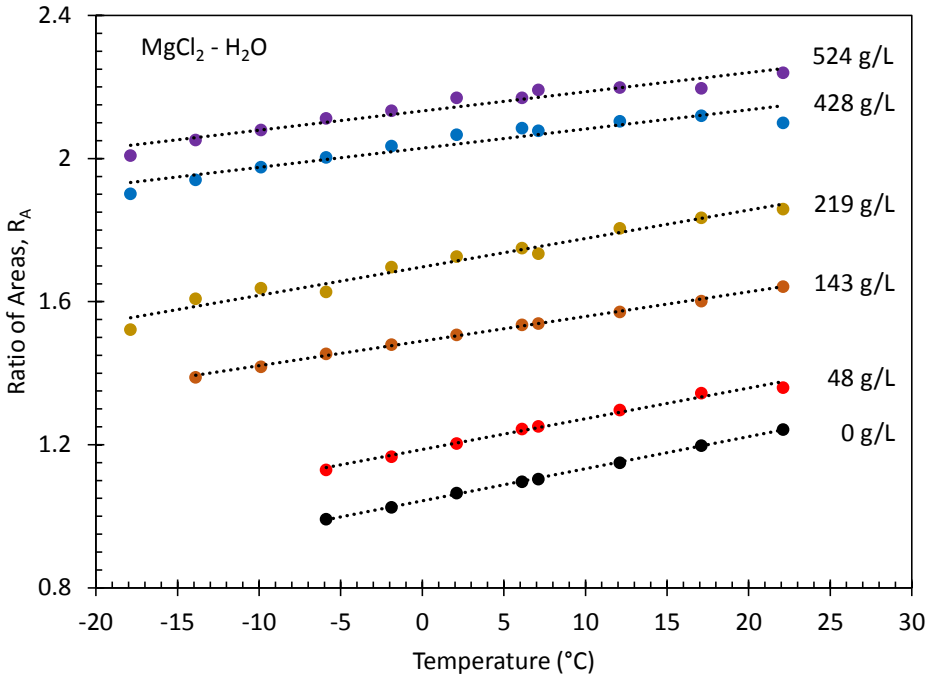

Figure 5.7: Benchmark plot created from the non-normalized Raman spectra of $MgCl_2$ solutions over a range of temperatures and concentrations.

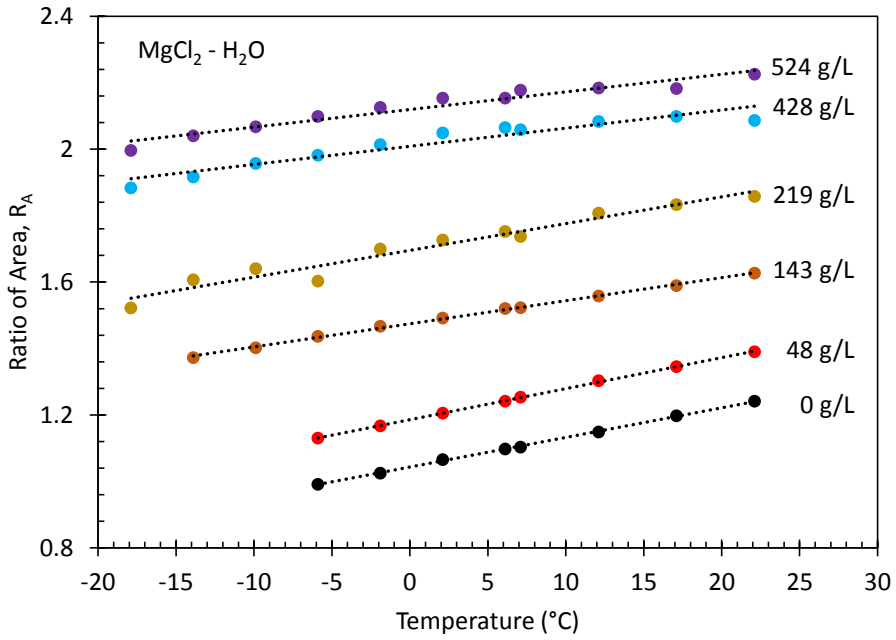

Figure 5.8: Benchmark plot created from the normalized Raman spectra of $MgCl_2$ solutions over a range of temperatures and concentrations.

5.2 Acetate Solutions

The KAc and CMA deicing salt's Raman spectra were subjected to a combination of Gaussian deconvolution-based peak subtraction and R_A calculations with unequal integration intervals to produce clear benchmark plots. When the acetate ion peaks are included in the R_A calculations, the benchmark plots become non-meaningful (Fig. 3.5). However, when the acetate ion peaks are removed from the stretching region of the water Raman spectrum (2800 to 3800 cm^{-1}) prior to performing R_A calculations, clear trends are present in the acetate solution benchmark plots like the chloride solution benchmark plots.

5.2.1 Benchmark Plots

The KAc non-normalized and normalized Raman spectra were used to create the benchmark plots in Figures 5.9 and 5.10 respectively. The plots display a noticeable difference between the trendlines on the non-normalized and the normalized KAc benchmark plots. The trendlines for the normalized KAc appear closer together and a few data points have clearly shifted their R_A value after the Raman spectrum has been normalized. This is caused by using unequal integration intervals for the R_A calculations. The normalization adds or subtracts area from both of the integration intervals which results in slightly different R_A values compared to the R_A values found for the non-normalized Raman spectra. The difference in R_A values between the non-normalized and the normalized benchmark plots can be seen in both the chloride and acetate salt solutions, but Gaussian deconvolution-based peaks subtraction makes the acetate spectra more susceptible to R_A variations after normalization. After peak subtraction, the polymer half of the Raman spectrum can have noise in the tail. This noise is amplified by the normalization process and can increase to a points

that it triggers a new wavenumber value for the integration limit (15% of maximum peak intensity), drastically changing the R_A value. Therefore, the R_A values for the KAc solutions vary more between the non-normalized and the normalized data compare to the chloride salt solution benchmark plots. While there is a difference between the benchmark plot for the non-normalized KAc Raman spectra and for the normalized KAc Raman spectra, the majority of the difference is caused by the normalization amplifying noise caused by the Gaussian deconvolution-based peak subtraction. Therefore, the non-normalized Raman spectra can be used to create the benchmark plots for the KAc solutions as with the chloride solutions because non-normalized benchmark plots clearly show the trends relating R_A to temperature over a range of concentrations.

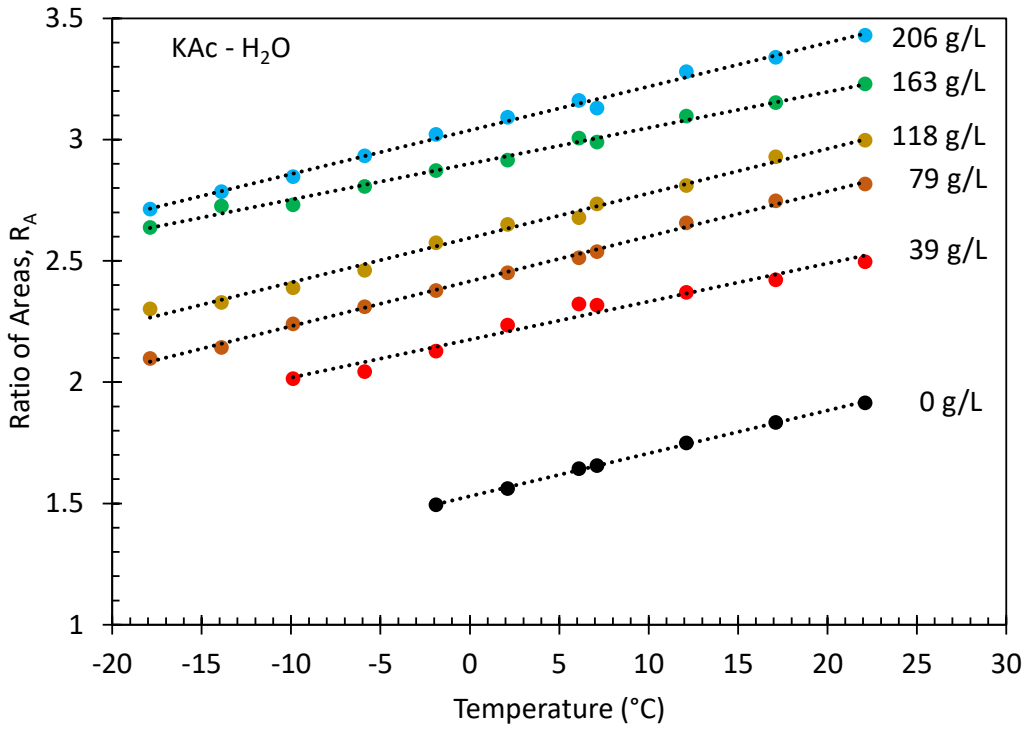

Figure 5.9: Benchmark plot of KAc solutions created using the non-normalized Raman spectra subjected to Gaussian deconvolution-based peak subtraction and R_A calculations.

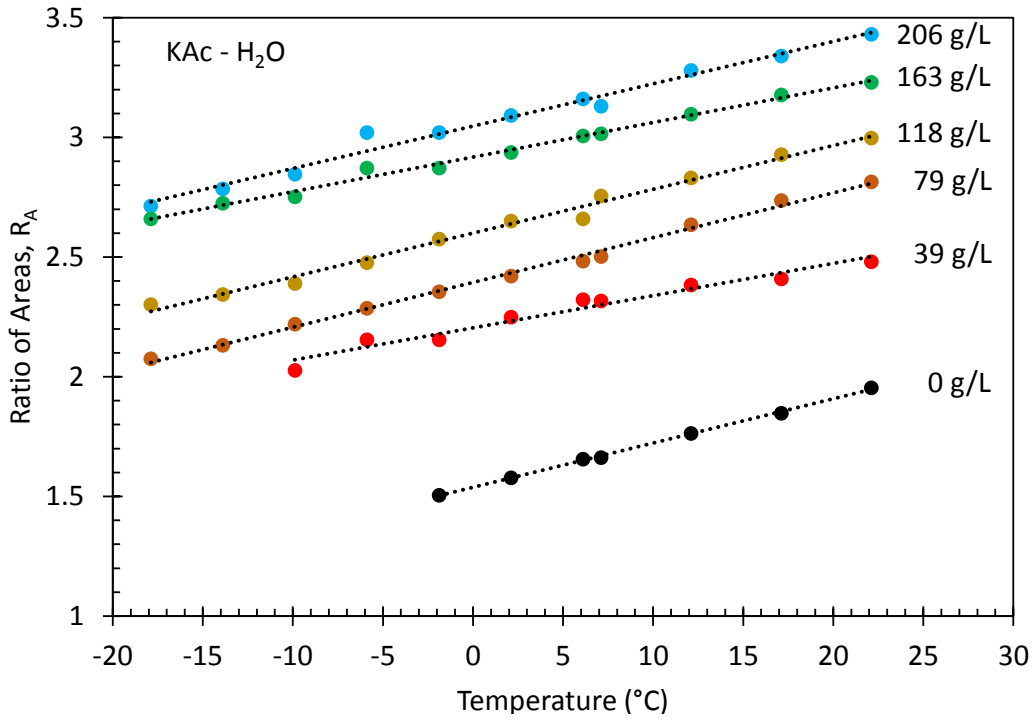

Figure 5.10: Benchmark plot of KAc solutions created using the normalized Raman spectra subjected to Gaussian deconvolution-based peak subtraction and R_A calculations.

The CMA benchmark plots were created using the non-normalized and the normalized CMA Raman spectra collected over a range of temperatures and concentrations (Fig. 5.11 and 5.12). Similar to the KAc benchmark plots, the CMA normalized benchmark plots begin to cluster when the trendlines are applied. In comparison, the non-normalized CMA Raman spectra benchmark plots present clearer and more evenly distributed trendlines that can clearly identify each salt concentration (Fig. 5.12).

Unlike the chloride based deicing salt benchmark plots, the acetate benchmark plots exhibit perceptible differences between the benchmark plots created using the non-normalized and the normalized Raman spectra. For the KAc solutions, as much as a 13% difference was seen between the non-normalized and the normalized bench-

mark plot data points though the average difference was 2%. Similarly, the CMA solutions experience as much as a 9% difference with an average of 4%. The percent difference between the non-normalized data and the normalized data benchmark plots is much greater for the acetate solutions compared to the NaCl which explains why the change in the trendlines can be determined without computer aid. While this difference is quite large, it is caused by the noise left behind by the Gaussian deconvolution-based peak subtraction. Again, it is clear that while normalizing the Raman spectra to an isosbestic point allows our data to be compared with previously published benchmark plots, the benchmark plots of the chloride and acetate solutions are less affected by the presence of noise when the non-normalized spectra are used.

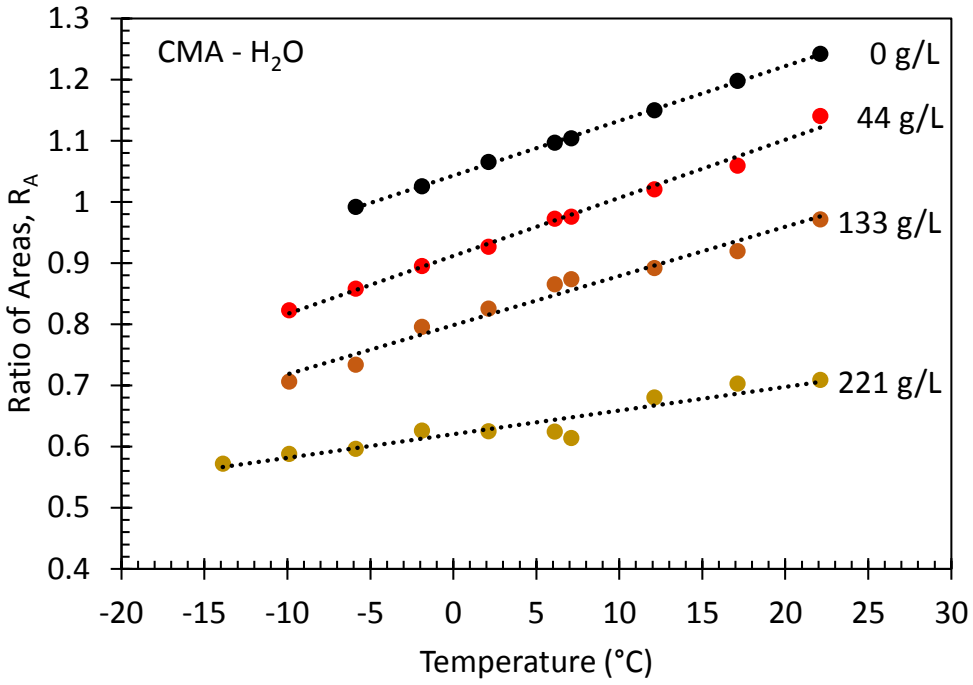

Figure 5.11: Benchmark plot of CMA solutions created using the non-normalized Raman spectra subjected to Gaussian deconvolution-based peak subtraction and R_A calculations.

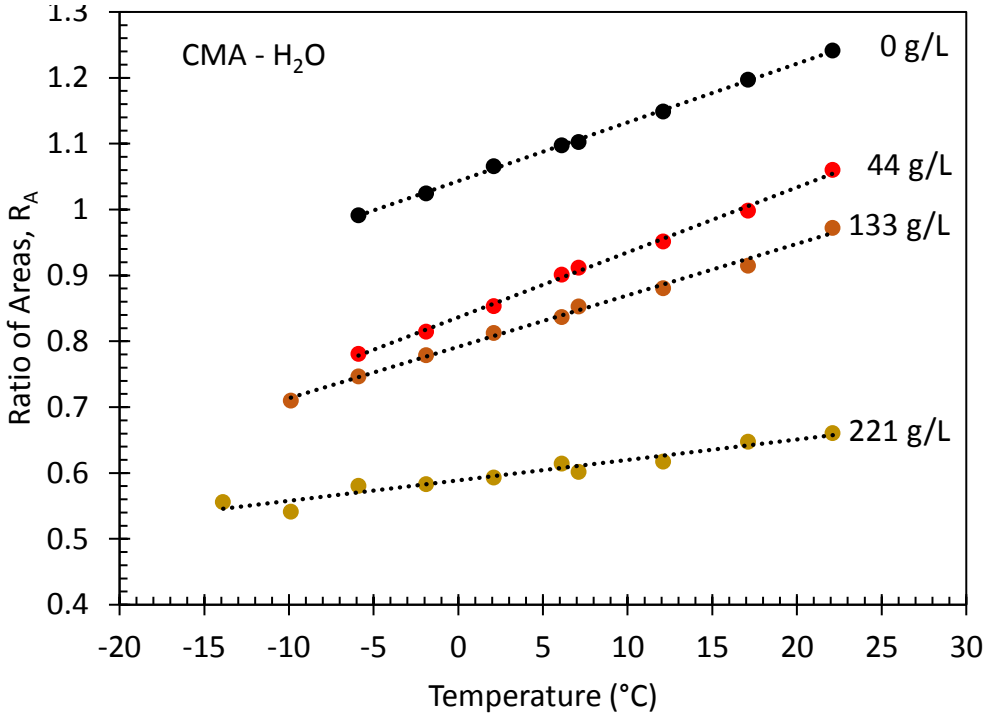

Figure 5.12: Benchmark plot of CMA solutions created using the normalized Raman spectra subjected to Gaussian deconvolution-based peak subtraction and R_A calculations.

5.3 Contaminated Sample Results

To complete the sample characterization tests, the effect of sand grains on the calculated concentration of a solution had to be quantified. The Raman spectrum for a eutectic concentration of NaCl was collected at 5 °C with and without sand grains and was plotted in Figure 5.13. With a close comparison of the water stretching region of the Raman spectra, it becomes apparent that the sand grains simultaneously increase the Raman intensity of the collected spectrum and increase the amount of fluorescence of the fiber optic material. It is hypothesized that both are caused by a larger amount of light reflecting back to the fiber optic probe. While a change in the Raman signal is apparent, possible changes in the calculated concentration cannot be determined by inspection alone.

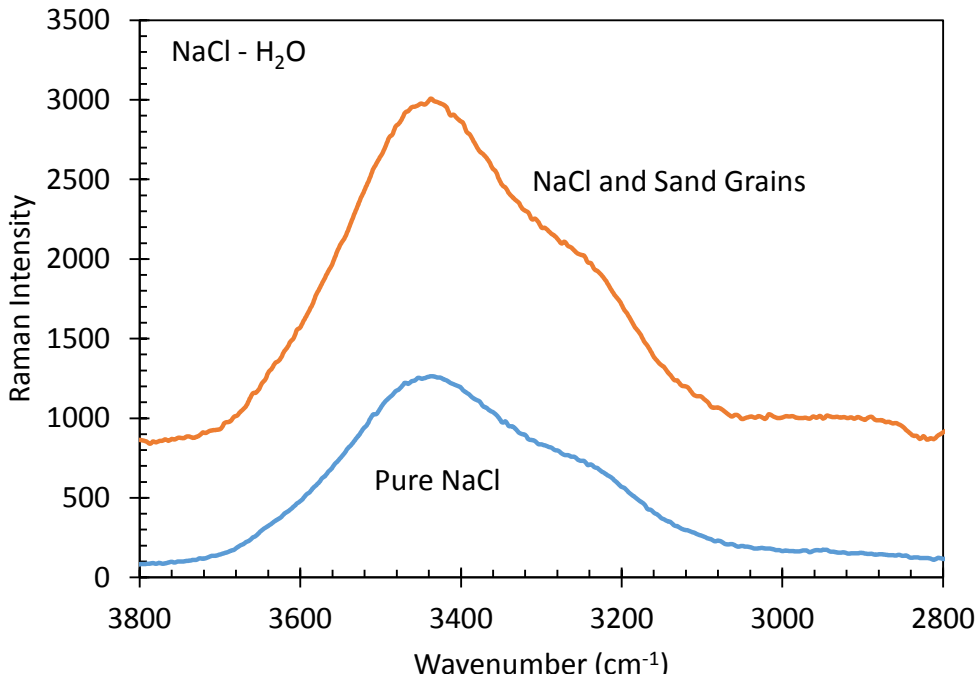

Figure 5.13: Close up of the Raman spectra for the contaminated sample and pure sample tested on a milled aluminum sample plate.

To determine the effect of the sand grains on the calculated concentration, the R_A calculations were applied to the non-normalized Raman spectra found with and without sand grains. Because of the large amount of fluorescence that the sand grains created in the Raman spectrum, the contaminated sample did not fall below 15% of the maximum peak intensity within the limits of the water stretching region (2800 to 3800 cm^{-1}). To compare the concentration calculations, the integration limits were altered for the contaminated sample so that the tail ends were included without incorporating the entire fluorescing region. This corresponded to using 30% for the start and end point for the R_A integration limits for the contaminated sample while 15% was used for the pure sample. Using the new integration limits, the contaminated sample had a R_A value of 1.84 while the pure solution had a R_A value of 2.24 which is a 20% difference. The NaCl non-normalized benchmark plot (Fig. 5.2) was used to determine the accuracy of the concentration calculations.

From the benchmark plot, the pure NaCl eutectic sample is slightly more concentrated than the eutectic concentration (234 g/L) used in this study. This was expected because the FHWA formula assumed the salt used in making the sample had up to 5% impurities while the salt used was 99% pure. Additionally, the contaminated sample calculation R_A value corresponds to a concentration value slightly less than 175 g/L. For the sample collected, the lowest integration value that was possible within the stretching region corresponds to 29% of the maximum peak intensity which gives an R_A value of 1.82 while choosing integration limits of 33% of the maximum peak intensity or greater results in an R_A value of 3.33 which corresponds to a sample more concentrated than the saturated mixture. Therefore, the integration limits used for the contaminated sample greatly change the calculated concentration. When the monomer and polymer peaks are chosen for the R_A calculations, the contaminated sample has a scalar ratio that corresponds to a weaker solution. Therefore, sand grains may cause the system to underestimate the concentration of salt currently on the roadway.

Because the solution with sand grains has fluorescence that causes the Raman spectrum to stay above 15% of the maximum peak intensity, the concentration of the solution is misrepresented. To work around this issue, the concentration of the solution will need to be compared to the concentrations calculated before and after. If the calculated concentration varies significantly (20% difference or more), it can be assumed that there are sand grains affecting the collected sample. Because the sample will be continuously changed as the tires move across the roadway, there is a small chance that the samples will all have sand grains in the view of the fiber optic probe; therefore, the proposed integration limits should be applied.

5.4 Varying Surfaces

To determine the effect of the testing surface on the concentration calculated from the Raman spectrum, the Raman spectra were collected for deionized water samples on testing surfaces with varying treatments. Additionally, the surfaces were then tested under varying orientations to determine how the testing surface orientation affects the calculated concentration.

Before testing, it was recorded that the as-cut sawn sample had unidirectional grooves across its surface while the sanded samples had an isotropic surface left behind during the sanding process. The grooves retained contaminants that entered the solution during testing. Several iterations of the tests were performed after cleaning the samples which revealed that the solution was more concentrated than a pure water sample, but less concentrated than the lowest 58 g/L NaCl solution. Nevertheless, the change in the maximum intensity of the Raman signal could be compared along with the amount of fluorescence to determine the change in the concentration calculation.

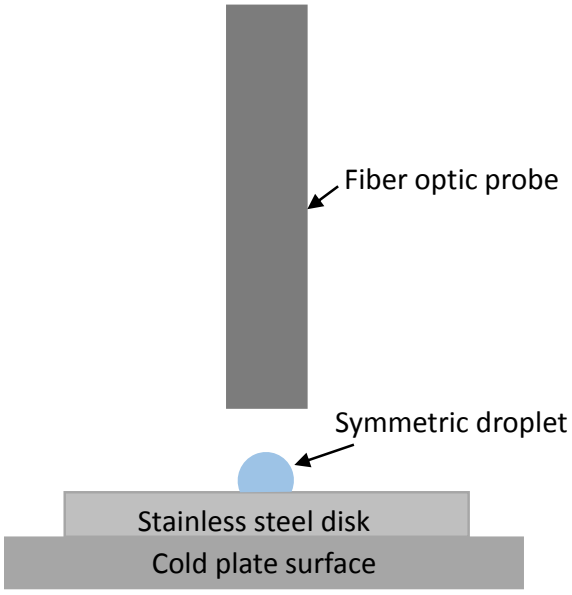

Figure 5.14: Pictorial representation of the fiber optic probe aligned perpendicularly with the stainless steel disk sample positioned horizontal on the cold plate surface.

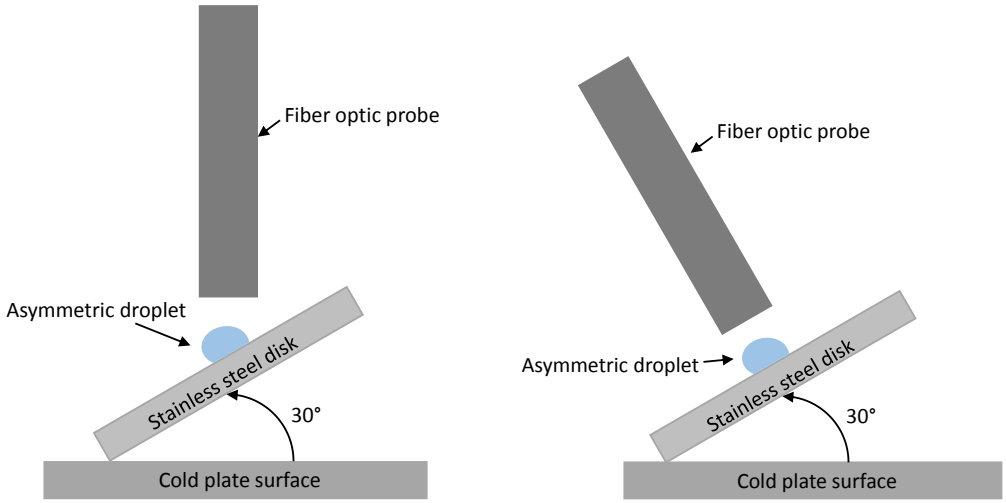

Figure 5.15: Pictorial representation of the stainless steel disk surface inclined at a 30° angle relative to the cold plate surface with the probe aligned (a) perpendicular to the cold plate and (b) perpendicular to the stainless steel disk.

As the orientation of the sample surface was varied throughout the tests, the height of the water droplets changed which altered the depth of the sample that the excitation laser interacted with. As a result, the inclined surfaces (Fig. 5.15) had lower Raman intensity as compared to the horizontal surface depicted in Figure 5.14 (Table 5.1, 5.2, and 5.3). Additionally, for all three surfaces and three orientations whose Raman spectra are shown in Appendix A.2, the maximum intensity was less than that found in the sample characterization tests (about 2,000 Raman intensity) because the sample characterization tests used a 3 mm thick layer of sample. Even without the surface inclined, the maximum height of the water droplets sprayed on the surface was about 2.22 mm. With fewer water molecules to interact with, a lower quantity of light was altered in wavelength which results in a lower intensity of the signal. Despite the low Raman intensities, the R_A calculations were performed on the non-normalized Raman spectra.

Table 5.1: Comparison of the maximum Raman intensity values for various surface treatments when the sample is laying horizontal on the cold plate (Fig. 5.14).

Surface Treatment	**Texture**	**Fluorescence**	**Max Intensity**
Sawn Sample	Unidirectional	Yes	945
120 Grit Sample	Non-directional	Yes	977
240 Grit Sample	Non-directional	Yes	518

Table 5.2: Comparison of the maximum Raman intensity values for various surface treatments when the sample is laying at a 30° angle to the cold plate surface with the probe perpendicular to the cold plate surface (Fig. 5.15a).

Surface Treatment	**Texture**	**Fluorescence**	**Max Intensity**
Perpendicular Sawn Sample	Unidirectional	Yes	243
Parallel Sawn Sample	Unidirectional	Yes	281
120 Grit Sample	Non-directional	Yes	357
240 Grit Sample	Non-directional	Yes	346

Table 5.3: Comparison of the maximum Raman intensity values for various surface treatments when the sample is laying at a 30° angle to the cold plate surface with the probe perpendicular to the stainless steel sample surface (Fig. 5.15b).

Surface Treatment	**Texture**	**Fluorescence**	**Max Intensity**
Perpendicular Sawn Sample	Unidirectional	Yes	644
Parallel Sawn Sample	Unidirectional	Yes	439
120 Grit Sample	Non-directional	Yes	435
240 Grit Sample	Non-directional	Yes	640

With the deionized water droplets quantified, the effect of the sample testing surface treatment on the water Raman spectra could be determined. For each test the water droplet was applied and the Raman spectrum was collected for each surface and probe orientation. Throughout the tests, the ideal focal distance for the fiber optic probe was 4 mm, but this was difficult to obtain when the probe was perpendicular to the cold plate and the testing surface was inclined at 30° (Fig. 4.4a). The inability to easily obtain the desired focal distance decrease the Raman intensity for those

samples. While the decreased Raman intensity allows noise to have a larger effect on the calculations performed on the Raman spectra, the R_A calculations showed only a 0.01 difference in the R_A scalar value for each surface and orientation combination. The difference of 0.01 corresponds to a few g/L. Figure 5.16 demonstrates the difference in the collected Raman intensities for the different surface treatments with the surface inclined at 30° while the fiber optic probe remains perpendicular to the cold plate surface (Fig. 5.14. Fluorescence is present in each sample, but it has a larger effect on the concentration calculations performed on surfaces producing low Raman intensity signals.

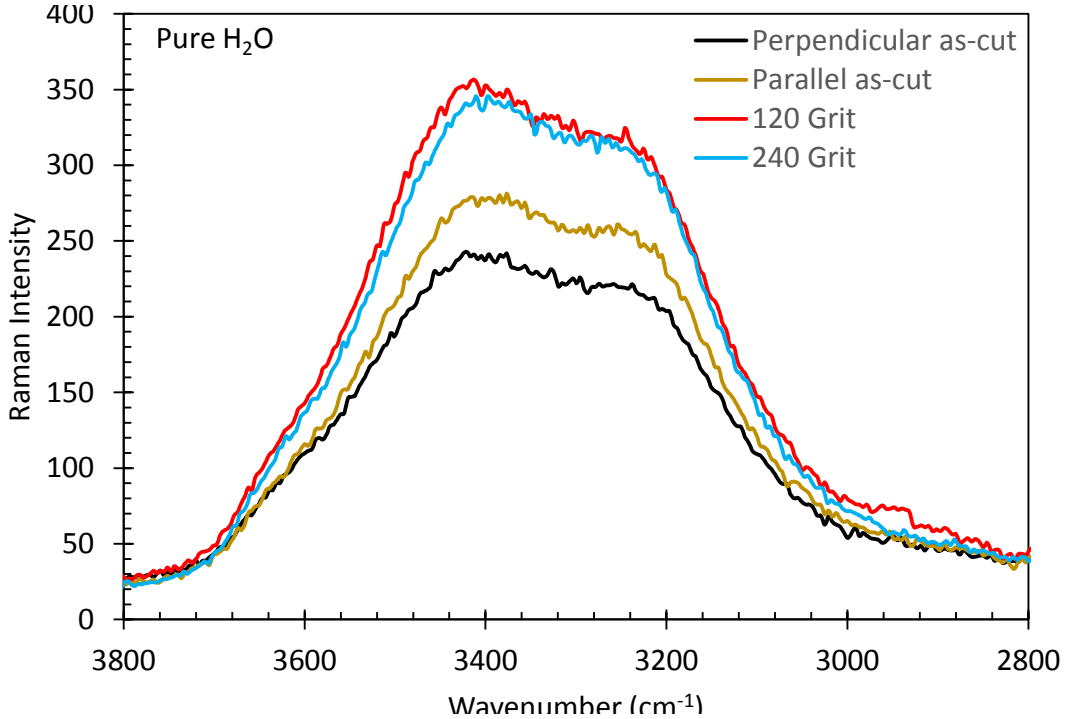

Figure 5.16: Comparison of the Raman spectra for the various sample treatments with the sample at a 30° angle from the cold plate surface and the probe perpendicular to the cold plate.

5.5 Discussion

This thesis project was performed to investigate the viability of using a Raman spectrometer as a vehicle mounted mobile salinity sensor. This was done by optimizing existing methods of determining the concentration of an aqueous solution from the collected Raman spectrum. The optimized method took the existing ratio of key integrated spectral area calculations, R_A, previously shown to work with aqueous chloride salt solutions and applied it to both chloride and acetate aqueous salt solutions. The R_A calculations are commonly implemented with equal integration intervals [36, 39, 42]. However, through iterations of calculations with varying integration limits, we found that the most consistent results were found when the start and end points were set to 15% of the maximum peak intensity of the collected Raman spectrum. This optimized method can compute the concentration of a chloride solution in seconds on a standard desktop accurately and consistently. Additional computing time is required to analyze aqueous acetate solutions with the same accuracy though. Directly applying existing R_A calculations to the acetate solution Raman spectra produces indecipherable benchmark plots due to the additional peaks that the acetate ions contribute to the stretching region of the water Raman spectrum.

Gaussian deconvolutions of the entire stretching region of the water Raman spectrum requires a lengthy computing time to achieve a satisfactory r^2 value. As a result, a hybrid method incorporating Gaussian deconvolution-based peak subtraction and R_A calculations was performed for the acetate aqueous solutions. This hybrid method subtracts the acetate ions' influence from the stretching region and produces accurate and consistent benchmark plots for the acetate solutions. While this hybrid approach does add additional computing time compared to a pure R_A approach, it can be performed in a few minutes on a standard desktop and produces useful benchmark plots for acetate solutions.

The R_A and hybrid Gaussian deconvolution and R_A calculations were performed on both the non-normalized Raman spectra and the Raman spectra normalized to an isosbestic point with 1,000 Raman intensity. The benchmark plots created for the chloride salts with both the non-normalized and normalized spectra show marginally different data point values, but the trends relatively unchanged. In contrast, the benchmark plots for the acetate solutions show perceptible changes to the data points and in the trendlines between the plots created with the non-normalized and those created with the normalized Raman spectra. The changes are a result of residual influence of the acetate ions being amplified during the normalization of the data. If equal integration intervals were used in the R_A calculations, the normalization would not affect the R_A values, but the normalization instead amplifies the area of one interval more than the other, resulting in a change in the R_A value. Because the non-normalized Raman spectra produce clear trends, the normalization is not required, unless the data is being compared to previously published reports. Therefore, the normalization can be removed from the data processing procedure which reduces the computation time even further.

Throughout this study, the Raman intensity of the collected spectra varied between tests. This was caused by adjusting the fiber optic probe's focal distance with each setup change to achieve the maximum signal intensity. As a result, no clear isosbestic point is found for the collected Raman spectra and, therefore, the true isosbestic point cannot be chosen as the midpoint for the R_A calculations. Instead, the isosbestic point defined by Đuričković and coworkers (3325 cm^{-1}) was used in the R_A calculations to closely compare results and because the value is in the accepted isosbestic wavenumber range [36]. While the isosbestic point locations could not be verified through this study, arbitrarily choosing a midpoint wavenumber for the R_A calculations between the polymer and monomer peaks has been proven as a valid ap-

proach [39, 42]. Therefore, the approach taken is valid whether the chosen midpoint value aligns with the isosbestic point or if it is an arbitrary value between the two main peaks.

To verify the concentration of the samples used throughout this study, the results of a 120 g/L solution were compared with data previously published by Đuričković and coworkers. The results were compared by testing the sample concentration sample with the same analysis technique (equal integration interval R_A calculations with subintervals one wavenumber in length). The trendlines show that the slope of the data points nearly match, but there is a slight offset in the y-intercepts of the data sets. The maximum difference between Đuričković and coworkers data points and ours is 4% which is within their reported concentration accuracy (5%). Because the concentration of our solution was verified through mass calculations, a conductivity probe, and an ICP-MS machine, the difference is unlikely to be caused by our concentration. The difference can possibly be explained in three ways: a difference in the isosbestic point, the R_A integration parameters, or the excitation laser power. If our data set had a different isosbestic point wavelength value, performing the R_A with the same midpoint could favor either the monomer or polymer peak more heavily which would result in either a higher or lower ratio scalar value. Moving the point slightly to either side of Đuričković and coworkers' isosbestic point value could allow our data to match theirs. This was not performed because our data did not present a clear isosbestic value. Additionally, if the R_A calculations do not have the exact same integration intervals and subintervals, the concentration calculations can differ. For example, performing Đuričković and coworkers' R_A technique with a finer numerical integration (subintervals a quarter of a wavenumber in length), there is as much as a 15% difference. Therefore, though care was taken to ensure that the same integration subintervals were used, the values were interpolated to compare which could have

caused some error. Lastly, the difference could be caused by the fact that this study used a 10 mW laser while Đuričković and coworkers implemented a 25 mW laser [36]. Mernagh and coworkers remarked that the power of the excitation laser should be reduced to avoid heating the sample which could cause the sample to appear more concentrated in the R_A calculations [39]. Comparing Đuričković and coworkers' previously published data against ours in a benchmark plot, Đuričković and coworkers' solution appears to be more concentrated than the corresponding sample tested in this study. Regardless of the difference, if the same excitation laser power, integration midpoint, and integration intervals and subintervals are maintained for all the collected Raman spectra for the R_A calculations, clear benchmark plots will be present as shown through this study and previously published studies.

After demonstrating the validity of using Raman spectroscopy to determine the concentration of an aqueous solutions containing one of the five most common salt deicers, a contaminated sample was tested with sand particles in the solution. The contaminated sample test shows that the sand particles do not drastically decrease the Raman intensity or introduce noise to the collected Raman signal. In some cases, the collected Raman intensity was increased by the presence of sand particles which caused fluorescence of occur in the fiber optic probe material while increasing the maximum peak intensity. Performing R_A calculations on the contaminated sample Raman spectrum revealed that the integration limits for the pure NaCl sample could not be implemented because of the large amount of fluorescence. Adjusting the limits of integration to ignore the fluorescence caused the concentration of the sample to appear as lower than the sample without sand grains. This occurred because the monomer and polymer halves have different slopes, so a change in the integration limits allows the area of one side to change more drastically than the other. Therefore, if sand grains are included in the sample, a different percentage of the maximum peak

intensity should be used as the integration limits, or using the original integration limits, the value should be compared to previously recorded concentration values. Because the contaminated sample may appear less concentrated than the true roadway precipitation concentration, it can either be taken as a conservative estimate, or the value can be filtered out.

Once the sample concentrations were determined for each aqueous salt solution with a milled aluminum plate sample surface, the effect of the sample surface on the calculated concentration could be determined. The tests involving three stainless steel samples with various surface treatments showed that the sanded and as-cut sawn stainless steel surfaces experienced about the same fluorescence of the Raman spectra as the milled aluminum sample dimple. This means that both the aluminum and the stainless-steel samples reflected light that caused fluorescence of the fiber optic material. Because the fluorescence is difficult to prevent when using a probe made of fiber optic material, it is better to choose a sample surface that increases the maximum intensity of the collected Raman spectrum. In doing so, the R_A calculations will be less affected by the presence of fluorescence in the signal. Therefore, the final Raman spectrometer mobile salinity sensor should employ a testing surface that reflects light back to the probe to achieve the maximum Raman intensity. Additional surfaces and surface treatments need to be performed to further verify this.

In addition to the testing surface treatment, the angle of the testing surface relative to the cold plate and the fiber optic probe was varied throughout the surface characterization tests for this study. The results of the tests show that the angle at which the excitation laser impinges on the testing surface has a greater effect on the Raman spectrum than the angle that the surface is inclined at relative to the ground. This means that the thickness of the solution droplet when it is inclined does not affect the collected Raman signal intensity compared to the effect of the angle of

the excitation laser reflecting off the testing surface. If the fiber optic probe causes the excitation laser to impinge perpendicularly on the testing surface, the maximum Raman intensity signal can be collected and the water Raman signal can be analyzed with less influence from noise and fluorescence of the probe material. When the laser interacts with the testing surface at an angle, less light is reflected to the probe which reduces the chances of fluorescence and, consequently, decreases the signal intensity to a level where noise affect concentration calculations. Despite the decreased intensity and chance for noise to interfere, the R_A values for the surface with the laser impinging on it at a 30° angle were only 0.01 $R_A$different than the R_A values for the surfaced with the probe perpendicular to the surface. This correlated to a difference of a few g/L. Additionally, the calculated concentration values for the stainless-steel samples was slightly higher than the deionized water concentration. This could be caused by two issues. The surfaces were treated and left with visible scratches (as desired for the sandpaper Grit used) which could have collected impurities that entered the deionized water sample during the test. Additionally, the stainless-steel samples experienced the same or less fluorescence than the samples tested in the aluminum milled plate. The fluorescence often has a slightly stronger effect on the polymer portion of the water Raman spectrum and increases its area slightly more than the area of the monomer. In doing so, the R_A value calculated from a sample with fluorescence will be lower than that of a sample collected without fluorescence. Therefore, samples tested on surfaces causing less fluorescence of the fiber optic probe will appear more concentrated than samples tests on surfaces that cause more fluorescence. Clearly, it is important to determine the amount of fluorescence cause by the chosen testing surface so that the appropriate benchmark plots can be used to determine the concentration of the unknown sample.

5.6 Summary

The tests performed in this study were designed to investigate the viability of using Raman spectroscopy to determine the concentration of deicing salt on the roadway in near real time. The R_A calculations performed in this study were optimized from previously published versions to work with both chloride and acetate solutions. The R_A calculations can be performed in a matter of seconds on a standard desktop for chloride salt solutions, but a hybrid Gaussian deconvolution and R_A approach is required to determine the concentration of an acetate solution. The hybrid approach takes a few minutes to perform; however, the approach is more consistent than applying R_A calculations to the acetate Raman spectra and is still faster than a full Gaussian deconvolution of the entire water stretching region of the Raman spectrum. Additionally, R_A calculations were performed on both the non-normalized and the normalized Raman spectra for each solution; however, the benchmark plots reveal that the trends remain the same for the non-normalized and the normalized plots. As a result, the normalization calculations can be removed from the data processing procedure which reduces the calculation time even further.

Using the optimized R_A calculations and the hybrid approach, clear benchmark plots can be created for both chloride and acetate solutions. Using the benchmark plots, our data can easily be compared to previously published results as well as used to determine the concentration of a sample with an unknown concentration when the salt and temperature are known. Comparing the previously published papers shows that the relationships between the R_A values, the concentration, and the temperature are still accurately present in the optimized method.

Additional tests performed in this study demonstrated that the testing surface and possible contaminations of the solution will affect the calculated concentration of the solution slightly. The presence of sand grains in the solution can increase

the maximum peak intensity of the Raman signal, but they can also increase the amount of fluorescence occurring from the fiber optic material. The percentage of the maximum peak intensity would need to be adjusted to compensate for this. Testing various sample surface treatments revealed that the surface treatment and orientation that results in the maximum Raman intensity should be used, but additional tests are required to state what treatment will produce the best results. However, the surface used for the tests should be recorded to ensure that the characteristics of the Raman signal are the same as the characteristics experience when the benchmark plot was made. If the benchmark plot was created with a surface experiencing more fluorescence, the concentration of the unknown solution may appear weaker than the true concentration of the sample.

Chapter 6

Conclusion

The FHWA, NDOT, and other state and local transportation agencies across the United States are perpetually investigating new methods for determining the concentration of deicing salt on the roadway in real-time to prevent over-salting the roadway. Methods exist for determining the concentration of a roadway precipitation sample, but few have the advantages that Raman spectroscopy provides: requiring a small sample size, no contact, and a relatively short concentration calculation time. This thesis was performed to investigate that Raman spectroscopy is a viable option for a mobile salinity sensor. In implementing a vehicle mounted mobile salinity sensor, the concentration of residual deicing salt will be measurable which will allow agencies to adjust the amount they apply accordingly. This will prevent undue stress on the environment and ensure that winter maintenance budgets are allocated appropriately.

One advantage of Raman spectroscopy is its ability to analyze an aqueous salt solution without processing the salt out of the sample. The disassociated salt ions interrupt the interactions between the water molecules which create shifts in the water Raman spectrum much like the shift created by varying the temperature of the sample. For this reason, the Raman spectrum were collected for samples over a

range of temperatures and salt concentrations for each of the five most common salt deicers.

Multiple methods exist for determining the concentration of an aqueous salt solution from the shifts that salt ions create in the water Raman spectrum. Most of these methods involve either a ratio analysis of key integrated spectral areas, similar to R_A, or Gaussian deconvolution of the stretching region of the water Raman spectrum. A fully unconstrained, six peak Gaussian deconvolution of the stretching region can take up to an hour to perform on a standard desktop. For this reason, this thesis focused on optimizing previously published methods to provide accurate and consistent results in near-real time for all five of the most common deicing salts.

The optimized method used to create the benchmark plots for this study centered around R_A calculations that could be performed in near real time. Because R_A calculations are commonly applied to chloride based aqueous solutions, they are susceptible to error when the acetate ion peaks are present. For this reason, the R_A calculations were combined with Gaussian deconvolution to subtract the acetate ion peaks and produce scalar values which then create meaningful benchmark plots. Though the hybrid approach using R_A calculations and Gaussian deconvolution does take a few minutes to perform, it creates benchmark plots that can be used to identify the concentration of an unknown acetate solution. Therefore, the optimized methods created in this study provide a method of determining the concentration of acetate and chloride salt solutions on the roadway in near real time.

Using the benchmark plots created for the acetate and chloride based aqueous solutions, the effect of the testing surface on the calculated concentration was investigated. Additional testing is required to create a list of surfaces and surface treatments that provide the best Raman signal with a high intensity and low fluorescence value. The tests performed showed that the best results are achieved when the fiber op-

tic probe is perpendicular to the testing surface though concentration results can be achieved when the fiber optic probe allows the laser to impinge upon the testing surface at a 30° angle. Lastly, the surface tests showed that the lower the intensity of the Raman signal, the more fluorescence skews the R_A calculations. This results in an incorrect concentration value being reported. Therefore, the mobile salinity sensor should be designed with a testing surface that reflects a large portion of the excitation laser with the fiber optic probe perpendicular to the testing surface.

Throughout this thesis, the test setup for both the surface and sample characterization tests remained the same, but a change in the test setup could produce comparable results. Previously published works analyzing the Raman spectrum have often used a 514.5 nm laser to collect the Raman spectra. This study used a 532 nm laser and obtained similar concentration results, so the concentration calculations are not largely affected by a change in the wavelength of the excitation laser. Additionally, this thesis used an extended range grating provided by Thermo Scientific to record the entire stretching region of the water Raman spectrum as opposed to the full range grating which cuts off the tail end of the monomer peak at 3575 cm^{-1}. By cutting off the tail end, the integration limits cannot be set to 15% of the maximum peak intensity, so an equal integration approach should be applied as in previous studies. This will provide clear benchmark plots, but the results may be less consistent. Therefore, if variations of the setup are offered, the analysis method will only need to change if the grating is changed.

Chapter 7

Future Work

While the work done throughout this study stands alone in its contribution to analyzing the concentration of aqueous salt solutions, the analysis methods must be paired with a physical system and a user interface to function as a mobile Raman spectroscopy salinity sensor. The following subsections provide details on the scope of the project regarding the physical and user interface required to create a functioning system.

7.1 Physical System

To determine the concentration of salt solution on the roadway in near-real time, the analysis techniques developed in this study require a physical system to collect the Raman spectra. While the physical system can take many forms, certain components are required for the system to function as a mobile Raman spectroscopy salinity sensor.

The on-vehicle system will use a Raman spectrometer placed on either the salt spreader or a freeway service patrol vehicle. The Raman spectrometer will house an

excitation laser, filters, and laser grating which the customer can choose based on their applied analysis method. The excitation laser will interact with the sample and the resulting Raman spectra will be collected through a fiber optic probe. Because the fiber optic probe can read the Raman spectrum of an aqueous solution outside of the Raman spectrometer, there is flexibility in the way the sample is collected.

While previous studies have mentioned that the Raman spectrum of a solution can be determine directly from the roadway [48], it is more common for systems to collected samples from tire splash [24, 27]. Systems that collect tire splash are often housed in the wheel well area following the tire to protect the unit and collect the most amount of sample available. With the sample collected, the fiber optic probe can collect the Raman spectrum which can be relayed to a computer system on the vehicle. This computer system will then use the analysis methods developed in this thesis to determine the concentration of the collected sample by lining up the calculated ratio value with the benchmark plot for the solution. To do this, only a rough estimate of the chemical composition of the solution and the temperature of the sample are required.

If acetate solutions are applied to the roadway, the current analyses methods applied in this study will need a more than the general purpose Matlab code and a standard laptop. Using the current general purpose Matlab code developed by O'Haver [47], the Gaussian deconvolution-based peak subtraction and R_A calculations can take anywhere from 10 to 45 minutes depending on how many parameters are fixed during the Gaussian deconvolution. To optimize the concentration calculations for acetate solutions, the physical system could include a faster computer capable of optimizing 15 parameters separately or could use an optimized regression calculator designed specifically for a Gaussian deconvolution involving five to six peaks. In doing so, the physical system would be able to calculate the concentration of an

acetate solution in a matter of seconds. This would mean that acetate and chloride solution concentrations can be determined at the same rate.

7.2 User Interface

While the physical system can collect the Raman spectra and implement the analysis methods that determine the concentration of the roadway sample, a user interface needs to be designed to alert transportation agencies when additional salting is needed.

With the benchmark plots found throughout the analyses in this thesis, the computer of the physical system can compare the R_A scalar value and determine the concentration of the solution if the temperature is known. The computer can then determine whether that concentration of solution is above or below the eutectic concentration for the salt in the solution. The answer can be outputted in a Boolean format that can be used as a quick indicator. For example, a light on the dashboard may shine red when the system determines that the solution is below the eutectic concentration and salt needs to be applied while it might shine green when there is sufficient salt on the roadway. Additionally, combining this system with a GPS, all of the concentration values can be logged and plotted so that troublesome areas can be patrolled more vigilantly.

This user-friendly interface will immediately tell the driver of the truck whether or not more deicing salt needs to be applied. In doing so, over-salting and under-salting can be avoided which benefits both transportation agencies and the environment. By providing a binary out, the system is easier to implement which provides incentive for transportation agencies to incorporate it into their existing anti- and deicing methods.

7.3 Future Research

In addition to setting the configuration of the physical setup and designing the user interface to implement the analyses methods, a few more topics must be researched. These topics include, but are not limited to, analyzing how stand-off Raman spectroscopy affects the calculated concentration, characterizing the change in the Raman intensity for a solution on a substrate with varying surface texture, characterizing the Raman spectra when a combination of salts are applied to the roadway, and determining the concentration of a sample as it flows over the testing surface.

This study demonstrated that Raman spectroscopy can be used to determine the concentration of salt in a solution when the temperature of the solution is known. However, throughout this study, the fiber optic probe had to maintain a focal distance close of 4 mm in order to collect the Raman spectra. This distance is unrealistic for real world applications especially when the solution is collected from tire splash; therefore, stand-off Raman spectroscopy must be investigated in order to determine whether a high enough Raman intensity signal can be collected in order to accurately calculate the concentration. Through a series of tests, this study also demonstrated that surface texture does not affect the fluorescence of the fiber optic probe, so determining the surface texture that would provide the maximum Raman intensity would increase the reliability. With a higher Raman intensity, the fluorescence will have a decreased effect on the calculated concentration, resulting in a more accurate concentration reading.

Additionally, DOTs across the country often use a combination of deicing salts in their applications to get the environmental and temperature benefits of using acetate salts while maintaining the cost benefits of chloride deicing salts. Characterizing the change in the Raman spectrum due to a mixture of salts will allow the researcher to determine if the existing benchmark plots can be used or if additional analysis

methods are required. This research is only needed in areas subjected to multiple deicing salts. Lastly, the physical system will need to collect and dispose of roadway precipitation samples which will most likely involve the precipitation flowing over the testing surface as the Raman spectrum is recorded. To account for this, additional tests performed to calculate the concentration of a sample flowing over the testing surface is required. From the tests performed in this study, it is clear that only a droplet of water is required to analyzed the concentration. Therefore, these tests can either be performed by continuously spraying the surface or by placing the testing surface under a continuous flow of sample. Either way, the tests will provide information on how well these analyses perform under a dynamic test setup with the depth of solution varying.

Clearly, the results in this thesis have created new research questions within the field of mobile salinity sensing. While some research questions will need to be answered before subjecting the Raman spectrometer mobile salinity sensor to unknown environments, the majority of questions will allow the physical system to be optimized after implementation.

Bibliography

[1] Performance Analysis Division NDOT. *State of Nevada Transportation Facts and Figures 2012*. 2012. Available at https://www.nevadadot.com/home/showdocument?id=2417.

[2] Performance Analysis Division NDOT. *State of Nevada Transportation Facts and Figures 2013*. 2013. Available at https://www.nevadadot.com/home/showdocument?id=2413.

[3] Performance Analysis Division NDOT. *State of Nevada Transportation Facts and Figures 2014*. 2014. Available at https://www.nevadadot.com/home/showdocument?id=2407.

[4] Performance Analysis Division NDOT. *State of Nevada Transportation 2015 Facts and Figures*. 2015. Available at https://www.nevadadot.com/home/showdocument?id=2411.

[5] Performance Analysis Division NDOT. *State of Nevada Transportation Facts and Figure 2016*. 2016. Available at https://www.nevadadot.com/home/showdocument?id=6446.

[6] Maryland Department of Transportation. *Analysis of the FY 2016 Maryland Executive Budget, 2015*. 2015. Available at http://mgaleg.maryland.gov/pubs/budgetfiscal/2016fy-budget-docs-operating-J00B01-MDOT-State-Highway-Administration.pdf.

[7] Maryland Department of Transportation. Analysis of the fy 2017 maryland executive budget, 2016. Report, 2016. Available at http://mgaleg.maryland.gov/pubs/budgetfiscal/2017fy-budget-docs-operating-J00B01-MDOT-State-Highway-Administration.pdf.

[8] Minnesota Department of Transportation. 2015-2016 winter maintenance report: At a glance, 2016. Available at http://www.dot.state.mn.us/maintenance/pdf/winterMaintenanceAnnualReport-2015.pdf.

[9] Roderick W. Hoffman, Charles R. Goldman, Sherrell Paulson, and Gary R. Winters. Aquatic impacts of deicing salts in the central sierra nevada mountains, california1. 1981.

[10] R. L. McCrum. Calcium magnesium acetate and sodium chloride as highway deicing salts: a comparative study. *Materials performance*, 28(12):24–28, 1989.

[11] Daniel L. Kelting and Corey L. Laxson. Review of effects and costs of road de-icing with recommendations for winter road management in the adirondack park. Report, Adirondack Watershed Institute, 2010.

[12] U.S. Department of Transportation Federal Highway Administration. Snow and ice, 2017. Available at `http://www.ops.fhwa.dot.gov/Weather/weather_events/snow_ice.htm`.

[13] Committee on the Comparative Costs of Rock Salt and Calcium Magnesium Acetate (CMA) for Highway Deicing. Highway deicing: Comparing salt and calcium magnesium acetate. Report 0309051231, Transportation Research Board, 1991.

[14] Patrick C. Casey, Clarence W. Alwan, Christine F. Kline, Gregory K. Landgraf, and Kimberly R. Linsenmayer. Impacts of using salt and salt brine for roadway deicing. Report, 2014.

[15] M. A. Equiza, M. Calvo-Polanco, D. Cirelli, J. Se/ norans, M. Wartenbe, C. Saunders, and J. J. Zwiazek. Long-term impact of road salt (nacl) on soil and urban trees in edmonton, canada. *Urban Forestry and Urban Greening*, 21:16–28, 2017.

[16] Isabel A. Munck, Chandalin M. Bennett, Kim S. Camilli, and Robert S. Nowak. Long-term impact of de-icing salts on tree health in the lake tahoe basin: Environmental influences and interactions with insects and diseases. *Forest ecology and management*, 260(7):1218–1229, 2010.

[17] Stephen A. Ketcham, L. David Minsk, Robert R. Blackburn, and Edward J. Fleege. Manual of practice for an effective anti-icing program: a guide for highway winter maintenance personnel. Report, 1996. Available at `https://www.fhwa.dot.gov/reports/mopeap/eapcov.htm`.

[18] Meg Ragonese. Nevada department of transportation: Prepared for winter snow removal, 2015.

[19] NDOT Research Division. Newsletter winter 2008. Report, 2008.

[20] Tony McClellan, Paul Boone, and Melody A. Coleman. Maintenance decision support system (mdss): Indiana department of transportation (indot) statewide implementation final report for fy09. Report, 2009.

[21] Randy D. Down and Jay H. Lehr. *Environmental instrumentation and analysis handbook*. John Wiley and Sons, 2005.

[22] Miles B. Whitener. Apparatus and methods for detecting wet and icy conditions. Report, 1901.

[23] Patrick A. Leonhardt and Inc Energy Absorption Systems. Roadway freezing point monitoring system and method, 2006.

[24] N. W. Garrick, N. P. Nikolaidis, and J. Luo. A portable method to determine chloride concentration on roadway pavements. *The New England Transportation Consortium*, 2002.

[25] A. W. Adamson. *A Textbook of Physical Chemistry*. Academic, New York. 1973.

[26] Marta Ruiz-Llata, Pedro Martín-Mateos, José R. López, and Pablo Acedo. Remote optical sensor for real-time residual salt monitoring on road surfaces. *Sensors and Actuators B: Chemical*, 191:371–376, 2014.

[27] Hisashi Iwata, K. Yamamoto, Keiichi Nishiduka, Hideo Higashi, Shinichi Nakao, and Yoshiyuki Miyazaki. Development of an on-vehicle type salinity measurement sensor for controlling winter roadway surfaces. *International Journal of ITS Research*, 2(1):77–84, 2008.

[28] Tatiana Dolenko, Sergey Burikov, Alexey Sabirov, and Victor Fadeev. Remote determination of temperature and salinity in presence of dissolved organic matter in natural waters using laser spectroscopy. *EARSeL eProceedings*, 10(2):159–165, 2011.

[29] Sergei A. Burikov, Irina V. Churina, Sergei A. Dolenko, Tatiana A. Dolenko, and Victor V. Fadeev. New approaches to determination of temperature and salinity of seawater by laser raman spectroscopy. *EARSeL eProceedings*, 3(3):298–305, 2004.

[30] G. I. Metternicht and J. A. Zinck. Remote sensing of soil salinity: potentials and constraints. *Remote sensing of Environment*, 85(1):1–20, 2003.

[31] Ewen Smith and 1948 Dent, Geoffrey. *Modern Raman spectroscopy: a practical approach*. J. Wiley, Hoboken, NJ, 2005.

[32] Derek A. Long. *The Raman Effect: A Unified Treatment of the Theory of Raman Scattering by Molecules*. John wiley & sons, LTD, West Sussex, England, 2002.

[33] David Warren Ball. *The basics of spectroscopy*, volume 49. Spie Press, 2001.

[34] Paulo Cesar Morais, Sebastião William da Silva, Maria Aparecida Godoy Soler, and Norbert Buske. Raman spectroscopy in magnetic fluids. *Biomolecular engineering*, 17(2):41–49, 2001.

[35] Dubravko Risović and Krešimir Furić. Comparison of raman spectroscopic methods for the determination of supercooled and liquid water temperature. *Journal of Raman spectroscopy*, 36(8):771–776, 2005.

[36] Ivana Đuričković, Mario Marchetti, Rémy Claverie, Patrice Bourson, Jean-Marie Chassot, and Marc D. Fontana. Experimental study of nacl aqueous solutions by raman spectroscopy: Towards a new optical sensor. *Applied Spectroscopy*, 64(8):853–857, 2010.

[37] G. E. Walrafen, M. S. Hokmabadi, and W. H. Yang. Raman isosbestic points from liquid water. *The Journal of chemical physics*, 85(12):6964–6969, 1986.

[38] Ana Maria Pereira Neto and Oswaldo Sala. The effect of temperature and liclo4 in the water structure: a raman spectroscopy study. *Brazilian journal of physics*, 34(1):137–141, 2004.

[39] T. P. Mernagh and A. R. Wilde. The use of the laser raman microprobe for the determination of salinity in fluid inclusions. *Geochimica et Cosmochimica Acta*, 53(4):765–771, 1989.

[40] Ruihua Li, Zhanpeng Jiang, Shaoqi Shi, and Hongwei Yang. Raman spectra and 17 o nmr study effects of cacl 2 and mgcl 2 on water structure. *Journal of Molecular Structure*, 645(1):69–75, 2003.

[41] K. Furić, I. Ciglenečki, and B. Ćosović. Raman spectroscopic study of sodium chloride water solutions. *Journal of Molecular Structure*, 550(1-3):225–234, 2000.

[42] G. M. Georgiev, T. K. Kalkanjiev, V. P. Petrov, and Zh Nickolov. Determination of salts in water solutions by a skewing parameter of the water raman band. *Applied spectroscopy*, 38(4):593–595, 1984.

[43] G. E. Walrafen, Y. C. Chu, and G. J. Piermarini. Low-frequency raman scattering from water at high pressures and high temperatures. *The Journal of Physical Chemistry*, 100(24):10363–10372, 1996.

[44] G. E. Walrafen. Raman spectral studies of the effects of temperature on water structure. *The Journal of Chemical Physics*, 47(1):114–126, 1967.

[45] Qiang Sun, Lei Zhao, Nuo Li, and Jin Liu. Raman spectroscopic study for the determination of cl- concentration (molarity scale) in aqueous solutions: Application to fluid inclusions. *Chemical Geology*, 272(1):55–61, 2010.

[46] David M. Carey and Gerald M. Korenowski. Measurement of the raman spectrum of liquid water. *The Journal of chemical physics*, 108(7):2669, 1998.

[47] T. O'Haver. A pragmatic introduction to signal processing with applications in scientific measurement. Report, 2016. Available at `http://terpconnect.umd.edu/~toh/spectrum/TOC.html`.

[48] Ivana Durickovic, Mario Marchetti, Stephanie Poissonnier, Guillaume Casteran, Rachel Mansour, Nathalie Schweigert, and Benoit Mars. De-icer quantification and phase transition detection by raman spectroscopy, 2013.

Appendix A

Raman Spectra

The non-normalized Raman spectra collected for the contaminated samples and the surface characterization tests are shown in Sections A.1 and A.2.

A.1 Contaminated Sample

A.1.1 Pure NaCl

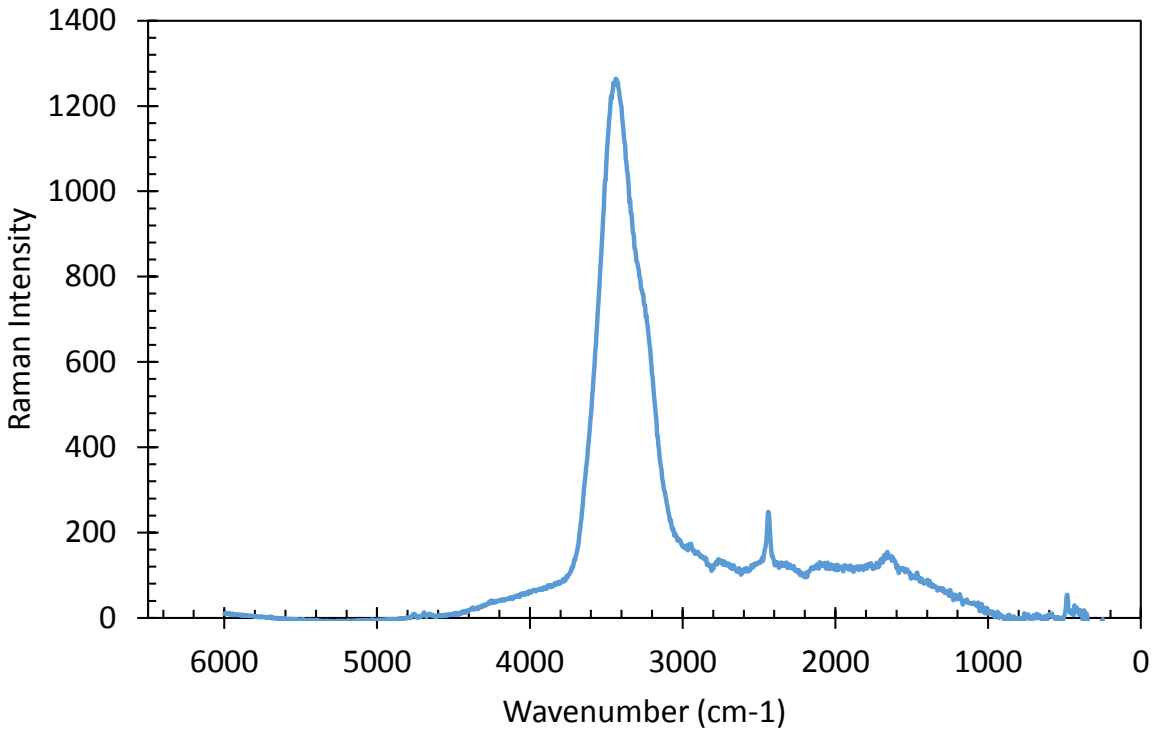

Figure A.1: Raman spectra for the pure NaCl solution to compare with the contaminated sample.

A.1.2 Contaminated Sample

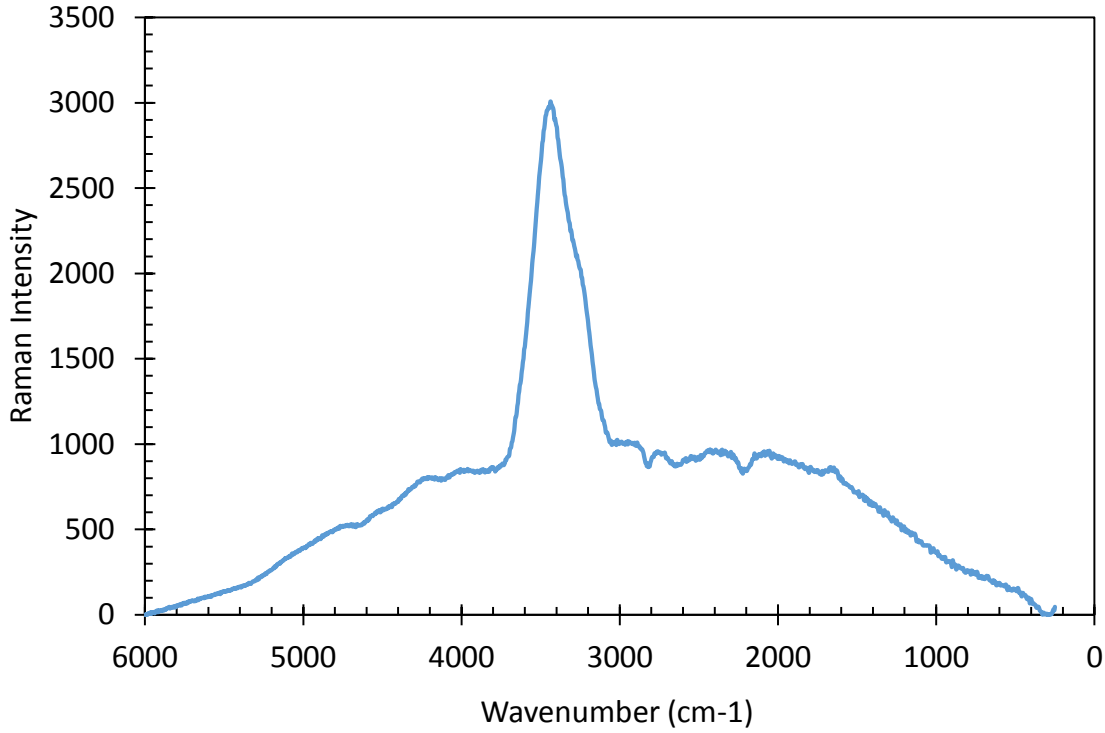

Figure A.2: Raman spectra for the contaminated NaCl solution with sand grains increasing the Raman intensity.

A.2 Surface Characterizations

A.2.1 Horizontal Stainless Steel Disk

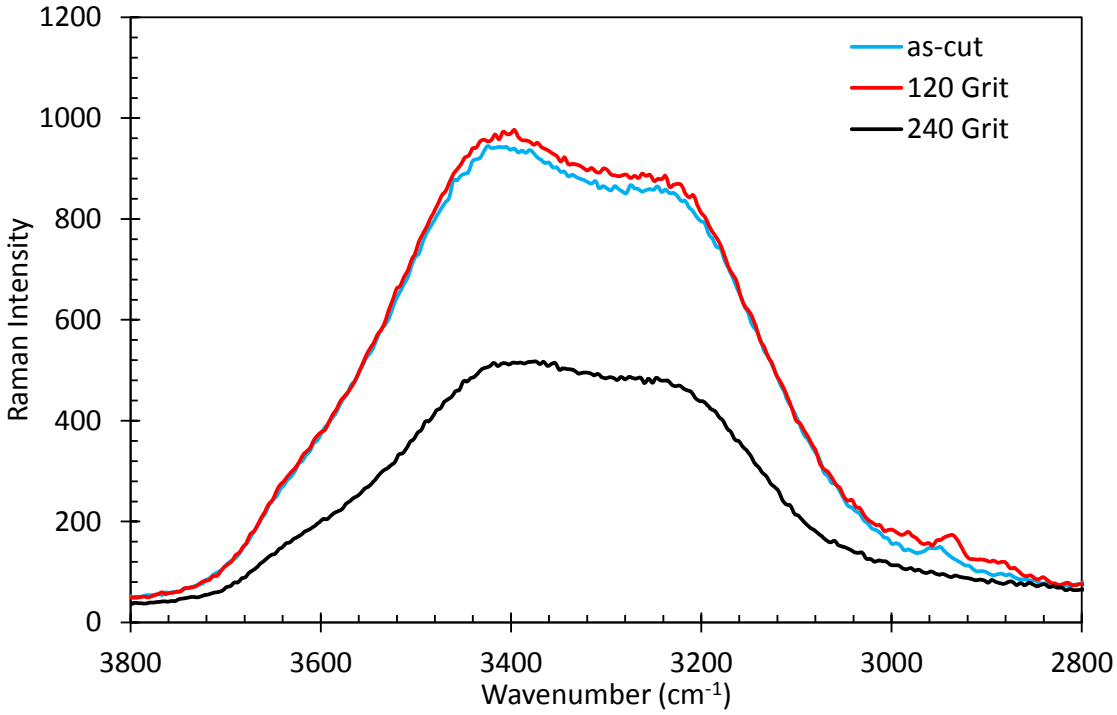

Figure A.3: Raman spectra for the stainless steel samples placed horizontal on the cold plate surface.

A.2.2 Stainless Steel Disk Inclined at 30°

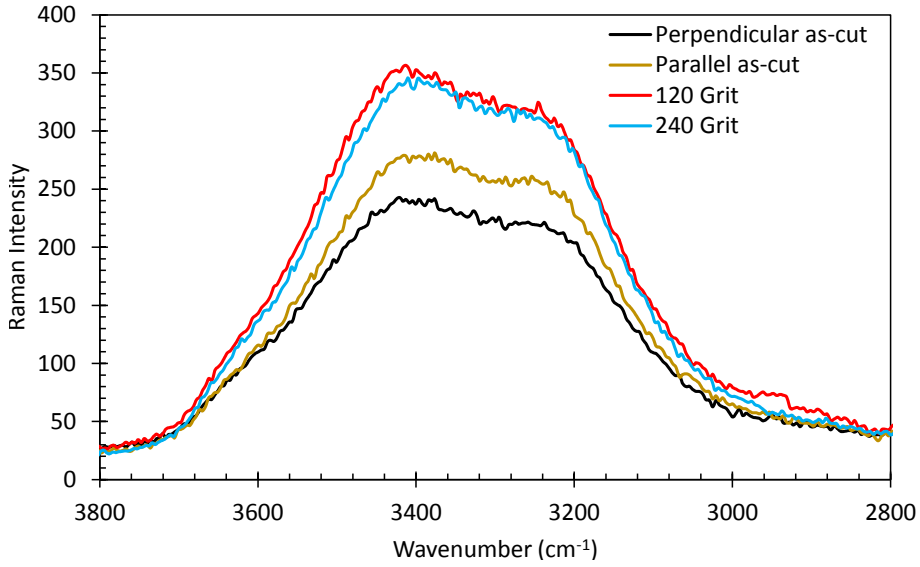

Figure A.4: Raman spectra for the stainless steel samples placed at a 30° angle relative to the cold plate with the fiber optic probe held perpendicular to the cold plate surface.

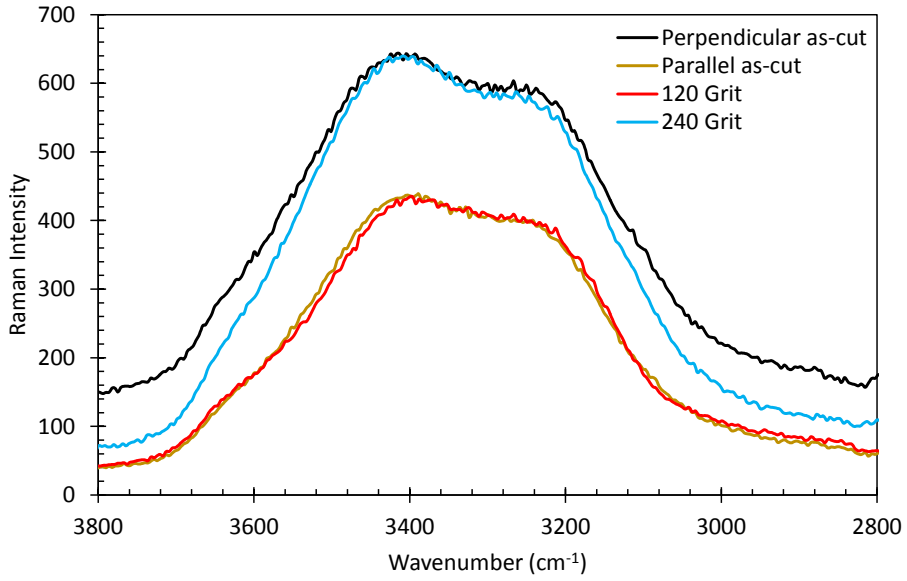

Figure A.5: Raman spectra for the stainless steel samples placed at a 30° angle relative to the cold plate surface with the fiber optic probe held perpendicular to the cold plate surface.

Appendix B

Matlab Files

B.1 Normalizing Raman Spectra to Isosbestic Point

```
% scale all isosbestic to 1000 intensity
clear all
clc

% read the Raman spectrum as the Raman spectrometer outputs it
N20 = 'N-0-+20_5.csv';
S20 = csvread(N20);
W20 = S20(:,1);


% determine the Raman intensity of the isosbestic point (3325 cm-1)
iso20 = min(find(ceil(S20(:,1)) == 3325));


% normalize the Raman spectra so that it has a value of 1,000 Raman
% intensity
for i = 1:1:length(S20)
    S20n(i,1) = S20(i,2)*(1000/S20(iso20,2));
end


% reconfigure the file with the new normalized spectra
normS20 = cat(2,W20,S20n);


```

```
% write a csv with the normalized spectra
csvwrite('normN-0-+20_5i.csv',normS20)
```

B.2 Ratio of the Areas

```
% ratio of areas,Ra, over various concentrations
clear all
clc
format compact

%reading the sample from the Raman spectrometer for each
    concentration
Sample351 = 'normN-6-10_4i.csv';
Sample292 = 'normN-5-16_5i.csv';
Sample234 = 'normN-4-20_4i.csv';
Sample175 = 'normN-3-16_6i.csv';
Sample120 = 'normN-120-14_3redoi.csv';
Sample117 = 'normN-2-16_3i.csv';
Sample58 = 'N-pure_plate_5.csv';
Sample0 = 'N-wsand_plate_5.csv';
s351 = csvread(Sample351); % 6M
s292 = csvread(Sample292); % 5M
s234 = csvread(Sample234); % 4M
s175 = csvread(Sample175); % 3M
s120 = csvread(Sample120); % 2M
s117 = csvread(Sample117); % 2M
s58 = csvread(Sample58); % 1M
s0 = csvread(Sample0); % 0M

% max peak intensity over the water streching region
max351 = max(s351(find(ceil(s351(:,1))==2700):find(ceil(s351
    (:,1))==3800),2));
max292 = max(s292(find(ceil(s292(:,1))==2700):find(ceil(s292
    (:,1))==3800),2));
max234 = max(s234(find(ceil(s234(:,1))==2700):find(ceil(s234
    (:,1))==3800),2));
max175 = max(s175(find(ceil(s175(:,1))==2700):find(ceil(s175
    (:,1))==3800),2));
max120 = max(s120(find(ceil(s120(:,1))==2700):find(ceil(s120
    (:,1))==3800),2));
max117 = max(s117(find(ceil(s117(:,1))==2700):find(ceil(s117
    (:,1))==3800),2));
max58 = max(s58(find(ceil(s58(:,1))==2700):find(ceil(s58(:,1)
```

```
    )==3800),2));
max0 = max(s0(find(ceil(s0(:,1))==2700):find(ceil(s0(:,1))
    ==3800),2));

% finding the isosbestic point for the Raman spectra
low351 = min(find(ceil(s351(:,1)) == 3325));
low292 = min(find(ceil(s292(:,1)) == 3325));
low234 = min(find(ceil(s234(:,1)) == 3325));
low175 = min(find(ceil(s175(:,1)) == 3325));
low120 = min(find(ceil(s120(:,1)) == 3325));
low117 = min(find(ceil(s117(:,1)) == 3325));
low58 = min(find(ceil(s58(:,1)) == 3325));
low0 = min(find(ceil(s0(:,1)) == 3325));

% finding the start and end points of the integration limits
    for each half
% 15% of max peak intensity
M351 = .15*max351;
tmp351 = abs(s351(:,2)-M351);
for i = 1:length(tmp351)
    if tmp351(i)<=8 % account for slight error in peak
        intensity
        ind351 = find(s351(:,2)==(-tmp351(i)+M351));
        if isnumeric(ind351)
            for n = 1:length(ind351)
                if s351(ind351(n),1) <3200 & s351(ind351(n)
                    ,1) >2700
                    index351_1(i) = s351(ind351(n),1);
                elseif s351(ind351(n)) <3800 & s351(ind351(n)
                    ) >(low351+1)
                    index351_2(i) = s351(ind351(n),1);
                end
            end
        else
        end

    indx351 = find(s351(:,2)==(tmp351(i)+M351));
        if isnumeric(indx351)
            for m = 1:length(indx351)
                if s351(indx351(m),1) <3200 & s351(indx351(m)
                    ,1) >2700
                    index351_1(i) = s351(indx351(m),1);
                elseif s351(indx351(m),1) <3800 & s351(
```

```
                    indx351(m),1) >(low351+1)
68                      index351_2(i) = s351(indx351(m),1);
69                  end
70              end
71          else
72          end
73      else
74      end
75  end
76
77  M292 = .15*max292;
78  tmp292 = abs(s292(:,2)-M292);
79  for i = 1:length(tmp292)
80      if tmp292(i)<=8
81          ind292 = find(s292(:,2)==(-tmp292(i)+M292));
82          if isnumeric(ind292)
83              for n = 1:length(ind292)
84                  if s292(ind292(n),1) <3200 & s292(ind292(n)
                        ,1) >2700
85                      index292_1(i) = s292(ind292(n),1);
86                  elseif s292(ind292(n)) <3800 & s292(ind292(n)
                        ) >(low292+1)
87                      index292_2(i) = s292(ind292(n),1);
88                  end
89              end
90          else
91          end
92
93      indx292 = find(s292(:,2)==(tmp292(i)+M292));
94          if isnumeric(indx292)
95              for m = 1:length(indx292)
96                  if s292(indx292(m),1) <3200 & s292(indx292(m)
                        ,1) >2700
97                      index292_1(i) = s292(indx292(m),1);
98                  elseif s292(indx292(m),1) <3800 & s292(
                        indx292(m),1) >(low292+1)
99                      index292_2(i) = s292(indx292(m),1);
100                 end
101             end
102         else
103         end
104     else
105     end
```

```
106 end
107
108 M234 = .15*max234;
109 tmp234 = abs(s234(:,2)-M234);
110 for i = 1:length(tmp234)
111     if tmp234(i)<=8
112         ind234 = find(s234(:,2)==(-tmp234(i)+M234));
113         if isnumeric(ind234)
114             for n = 1:length(ind234)
115                 if s234(ind234(n),1) <3200 & s234(ind234(n)
                        ,1) >2700
116                     index234_1(i) = s234(ind234(n),1);
117                 elseif s234(ind234(n),1) <3800 & s234(ind234(
                        n),1) >(low234+1)
118                     index234_2(i) = s234(ind234(n),1);
119                 end
120             end
121         else
122         end
123
124     indx234 = find(s234(:,2)==(tmp234(i)+M234));
125         if isnumeric(indx234)
126             for m = 1:length(indx234)
127                 if s234(indx234(m),1) <3200 & s234(indx234(m)
                        ,1) >2700
128                     index234_1(i) = s234(indx234(m),1);
129                 elseif s234(indx234(m),1) <3800 && s234(
                        indx234(m),1) >(low234+1)
130                     index234_2(i) = s234(indx234(m),1);
131                 end
132             end
133         else
134         end
135     else
136     end
137 end
138
139 M175 = .15*max175;
140 tmp175 = abs(s175(:,2)-M175);
141 for i = 1:length(tmp175)
142     if tmp175(i)<=8
143         ind175 = find(s175(:,2)==(-tmp175(i)+M175));
144         if isnumeric(ind175)
```

```
145                 for n = 1:length(ind175)
146                     if s175(ind175(n),1) <3200 & s175(ind175(n)
                            ,1) >2700
147                         index175_1(i) = s175(ind175(n),1);
148                     elseif s175(ind175(n),1) <3800 & s175(ind175(
                           n),1) >(low175+1)
149                         index175_2(i) = s175(ind175(n),1);
150                     end
151                 end
152             else
153             end
154
155         indx175 = find(s175(:,2)==(tmp175(i)+M175));
156             if isnumeric(indx175)
157                 for m = 1:length(indx175)
158                     if s175(indx175(m),1) <3200 & s175(indx175(m)
                            ,1) >2700
159                         index175_1(i) = s175(indx175(m),1);
160                     elseif s175(indx175(m),1) <3800 & s175(
                           indx175(m),1) >(low175+1)
161                         index175_2(i) = s175(indx175(m),1);
162                     end
163                 end
164             else
165             end
166         else
167         end
168 end
169
170 M120 = .15*max120;
171 tmp120 = abs(s120(:,2)-M120);
172 for i = 1:length(tmp120)
173     if tmp120(i)<=8
174         ind120 = find(s120(:,2)==(-tmp120(i)+M120));
175         if isnumeric(ind120)
176             for n = 1:length(ind120)
177                 if s120(ind120(n),1) <3200 & s120(ind120(n)
                        ,1) >2700
178                     index120_1(i) = s120(ind120(n),1);
179                 elseif s120(ind120(n),1) <3800 & s120(ind120(
                       n),1) >(low120+1)
180                     index120_2(i) = s120(ind120(n),1);
181                 end
```

```
182             end
183         else
184         end
185
186     indx120 = find(s120(:,2)==(tmp120(i)+M120));
187         if isnumeric(indx120)
188             for m = 1:length(indx120)
189                 if s120(indx120(m),1) <3200 & s120(indx120(m)
                        ,1) >2700
190                     index120_1(i) = s120(indx120(m),1);
191                 elseif s120(indx120(m),1) <3800 & s120(
                        indx120(m),1) >(low120+1)
192                     index120_2(i) = s120(indx120(m),1);
193                 end
194             end
195         else
196         end
197     else
198     end
199 end
200
201 M117 = .15*max117;
202 tmp117 = abs(s117(:,2)-M117);
203 for i = 1:length(tmp117)
204     if tmp117(i)<=8
205         ind117 = find(s117(:,2)==(-tmp117(i)+M117));
206         if isnumeric(ind117)
207             for n = 1:length(ind117)
208                 if s117(ind117(n),1) <3200 & s117(ind117(n)
                        ,1) >2700
209                     index117_1(i) = s117(ind117(n),1);
210                 elseif s117(ind117(n),1) <3800 & s117(ind117(
                        n),1) >(low117+1)
211                     index117_2(i) = s117(ind117(n),1);
212                 end
213             end
214         else
215         end
216
217     indx117 = find(s117(:,2)==(tmp117(i)+M117));
218         if isnumeric(indx117)
219             for m = 1:length(indx117)
220                 if s117(indx117(m),1) <3200 & s117(indx117(m)
```

```
                    ,1) >2700
221                     index117_1(i) = s117(indx117(m),1);
222                 elseif s117(indx117(m),1) <3800 & s117(
                        indx117(m),1) >(low117+1)
223                     index117_2(i) = s117(indx117(m),1);
224                 end
225             end
226         else
227         end
228     else
229     end
230 end
231
232 M58 = .12*max58;
233 tmp58 = abs(s58(:,2)-M58);
234 for i = 1:length(tmp58)
235     if tmp58(i)<=1
236         ind58 = find(s58(:,2)==(-tmp58(i)+M58));
237         if isnumeric(ind58)
238             for n = 1:length(ind58)
239                 if s58(ind58(n),1) <3200 & s58(ind58(n),1)
                        >2700
240                     index58_1(i) = s58(ind58(n),1);
241                 elseif s58(ind58(n),1) <3800 & s58(ind58(n)
                        ,1) >(low58+1)
242                     index58_2(i) = s58(ind58(n),1);
243                 end
244             end
245         else
246         end
247
248     indx58 = find(s58(:,2)==(tmp58(i)+M58));
249         if isnumeric(indx58)
250             for m = 1:length(indx58)
251                 if s58(indx58(m),1) <3200 & s58(indx58(m),1)
                        >2700
252                     index58_1(i) = s58(indx58(m),1);
253                 elseif s58(indx58(m),1) <3800 & s58(indx58(m)
                        ,1) >(low58+1)
254                     index58_2(i) = s58(indx58(m),1);
255                 end
256             end
257         else
```

```
258             end
259         else
260         end
261 end
262
263 M0 = .33*max0;
264 tmp0 = abs(s0(:,2)-M0);
265 for i = 1:length(tmp0)
266     if tmp0(i)<=8
267         ind0 = find(s0(:,2)==(-tmp0(i)+M0));
268         if isnumeric(ind0)
269             for n = 1:length(ind0)
270                 if s0(ind0(n),1) <3200 & s0(ind0(n),1) >2700
271                     index0_1(i) = s0(ind0(n),1);
272                 elseif s0(ind0(n),1) <3800 & s0(ind0(n),1) >(
                        low0+1)
273                     index0_2(i) = s0(ind0(n),1);
274                 end
275             end
276         else
277         end
278
279     indx0 = find(s0(:,2)==(tmp0(i)+M0));
280         if isnumeric(indx0)
281             for m = 1:length(indx0)
282                 if s0(indx0(m),1) <3200 & s0(indx0(m),1)
                        >2700
283                     index0_1(i) = s0(indx0(m),1);
284                 elseif s0(indx0(m),1) <3800 & s0(indx0(m),1)
                        >(low0+1)
285                     index0_2(i) = s0(indx0(m),1);
286                 end
287             end
288         else
289         end
290     else
291     end
292 end
293
294 % remove zeros from an array
295 index_351_1 = index351_1(index351_1~=0);
296 index_351_2 = index351_2(index351_2~=0);
297 index_292_1 = index292_1(index292_1~=0);
```

```
298 index_292_2 = index292_2(index292_2~=0);
299 index_234_1 = index234_1(index234_1~=0);
300 index_234_2 = index234_2(index234_2~=0);
301 index_175_1 = index175_1(index175_1~=0);
302 index_175_2 = index175_2(index175_2~=0);
303 index_120_1 = index120_1(index120_1~=0);
304 index_120_2 = index120_2(index120_2~=0);
305 index_117_1 = index117_1(index117_1~=0);
306 index_117_2 = index117_2(index117_2~=0);
307 index_58_1 = index58_1(index58_1~=0);
308 index_58_2 = index58_2(index58_2~=0);
309 index_0_1 = index0_1(index0_1~=0);
310 index_0_2 = index0_2(index0_2~=0);
311
312 for k = 1:1:4091 % perform the numerical integration
313 preSd351(k+1,1) = ((s351(k+1,2)+ s351(k,2))/2)*(s351(k+1,1)-
      s351(k,1));
314 preSd292(k+1,1) = ((s292(k+1,2)+ s292(k,2))/2)*(s292(k+1,1)-
      s292(k,1));
315 preSd234(k+1,1) = ((s234(k+1,2)+ s234(k,2))/2)*(s234(k+1,1)-
      s234(k,1));
316 preSd175(k+1,1) = ((s175(k+1,2)+ s175(k,2))/2)*(s175(k+1,1)-
      s175(k,1));
317 preSd120(k+1,1) = ((s120(k+1,2)+ s120(k,2))/2)*(s120(k+1,1)-
      s120(k,1));
318 preSd117(k+1,1) = ((s117(k+1,2)+ s117(k,2))/2)*(s117(k+1,1)-
      s117(k,1));
319 preSd58(k+1,1) = ((s58(k+1,2)+ s58(k,2))/2)*(s58(k+1,1)- s58(
      k,1));
320 preSd0(k+1,1) = ((s0(k+1,2)+ s0(k,2))/2)*(s0(k+1,1)- s0(k,1))
      ;
321 end
322
323
324 % numerator (monomer) = from 3326 to 15% of max peak
      intensity
325 % denomenator (polymer) = from 15% of max peak intensity to
      3325
326 Sd20_351_num = preSd351((low351+1):int64(min(index_351_2)),1)
      ;
327 Sd20_351_den = preSd351(int64(max(index_351_1)):low351,1);
328 Sd20_292_num = preSd292((low292+1):int64(min(index_292_2)),1)
      ;
```

```
Sd20_292_den = preSd292(int64(max(index_292_1)):low292,1);
Sd20_234_num = preSd234((low234+1):int64(min(index_234_2)),1)
    ;
Sd20_234_den = preSd234(int64(max(index_234_1)):low234,1);
Sd20_175_num = preSd175((low175+1):int64(min(index_175_2)),1)
    ;
Sd20_175_den = preSd175(int64(max(index_175_1)):low175,1);
Sd20_120_num = preSd120((low120+1):int64(min(index_120_2)),1)
    ;
Sd20_120_den = preSd120(int64(max(index_120_1)):low120,1);
Sd20_117_num = preSd117((low117+1):int64(min(index_117_2)),1)
    ;
Sd20_117_den = preSd117(int64(max(index_117_1)):low117,1);
Sd20_58_num = preSd58((low58+1):int64(min(index_58_2)),1);
Sd20_58_den = preSd58(int64(max(index_58_1)):low58,1);
Sd20_0_num = preSd0((low0+1):int64(min(index_0_2)),1);
Sd20_0_den = preSd0(int64(max(index_0_1)):low0,1);

% finding Ra for each concentration
Ra20_351 = sum(Sd20_351_num)/sum(Sd20_351_den)
Ra20_292 = sum(Sd20_292_num)/sum(Sd20_292_den)
Ra20_234 = sum(Sd20_234_num)/sum(Sd20_234_den)
Ra20_175 = sum(Sd20_175_num)/sum(Sd20_175_den)
Ra20_120 = sum(Sd20_120_num)/sum(Sd20_120_den)
Ra20_117 = sum(Sd20_117_num)/sum(Sd20_117_den)
Ra20_58 = sum(Sd20_58_num)/sum(Sd20_58_den)
Ra20_0 = sum(Sd20_0_num)/sum(Sd20_0_den)
```

B.3 Gaussian Deconvolution-Based Peak Subtraction

```
% Gaussian deconvolution based peak subtraction
clear all
clc
close all

% read the acetate solution Raman spectrum
K1s = 'K-2-19_5uni.csv';
K1 = csvread(K1s);
x1 = K1(:,1);

% recreating the gaussian peak that describes the lower
    wavenumber acetate
```

```
% peak
FWHM1 = 25.79;
sig1 = FWHM1/(2*sqrt(2*log(2)));
mean1 = 2935;
peak_max1 = 923.09;

% recreating the gaussian peak that describes the higher
    wavenumber acetate
% peak
FWHM1_2 = 184;
sig1_2 = FWHM1_2/(2*sqrt(2*log(2)));
mean1_2 = 2978.89;
peak_max1_2 = 282.69;

for i = 1:length(K1)
    y_calc1(i) = normpdf(x1(i),mean1,sig1);
    y_calc1_2(i) = normpdf(x1(i),mean1_2,sig1_2);
end

% subtracting the acetate peaks from the aqueous solution
    Raman spectrum
y1 = y_calc1*(peak_max1/max(y_calc1));
y1_2 = y_calc1_2*(peak_max1_2/max(y_calc1_2));

wave1 = K1(:,2)'-y1;
wave1_2 = wave1-y1_2;

% creating the file for the adjusted spectrum
subtwopeaks1 = cat(2,x1,wave1_2');
csvwrite('K-2-19_5uni_subconstwidth_old.csv',subtwopeaks1)


% Plotting all of the component Gaussian peaks from the data
    found using
% O'Haver's deconvolution tool for Matlab
FWHM1_3 = 231.43;
sig1_3 = FWHM1_3/(2*sqrt(2*log(2)));
mean1_3 = 3245;
peak_max1_3 = 752.2;

FWHM1_4 = 162.83;
sig1_4 = FWHM1_4/(2*sqrt(2*log(2)));
mean1_4 = 3392;
```

```
peak_max1_4 = 589.57;

FWHM1_5 = 181.26;
sig1_5 = FWHM1_5/(2*sqrt(2*log(2)));
mean1_5 = 3506;
peak_max1_5 = 687.81;

FWHM1_6 = 90.38;
sig1_6 = FWHM1_6/(2*sqrt(2*log(2)));
mean1_6 = 3636;
peak_max1_6 = 124.4;

for i = 1:length(K1)
    y_calc1_3(i) = normpdf(x1(i),mean1_3,sig1_3);
    y_calc1_4(i) = normpdf(x1(i),mean1_4,sig1_4);
    y_calc1_5(i) = normpdf(x1(i),mean1_5,sig1_5);
    y_calc1_6(i) = normpdf(x1(i),mean1_6,sig1_6);
end

y1_3 = y_calc1_3*(peak_max1_3/max(y_calc1_3));
y1_4 = y_calc1_4*(peak_max1_4/max(y_calc1_4));
y1_5 = y_calc1_5*(peak_max1_5/max(y_calc1_5));
y1_6 = y_calc1_6*(peak_max1_6/max(y_calc1_6));

hold on
plot(x1, K1(:,2), 'k-', x1, y1, 'g--', x1, y1_2, 'g--',x1,
   y1_3, 'g--', x1, y1_4, 'g--', x1, y1_5, 'g--', x1, y1_6, '
   g--')
plot(x1, wave1_2, 'b-','LineWidth',1.5)
```